# A case study of paleoenvironmental interactions during the Miocene Climate Optimum in southwestern Paratethys

Kopecká, Jitka; Holcová, Katarína; Brlek, Mihovil; Scheiner, Filip; Ackerman, Lukáš; Rejšek, Jan; Milovský, Rastislav; Baranyi, Viktória; Gaynor, Sean; Galović, Ines; Brčić, Vlatko; Belak, Mirko; Bakrač, Koraljka

**How to cite**

KOPECKÁ, Jitka et al. A case study of paleoenvironmental interactions during the Miocene Climate Optimum in southwestern Paratethys. In: Global and planetary change, 2022, p. 103784. doi: 10.1016/j.gloplacha.2022.103784

This publication URL: https://archive-ouverte.unige.ch/unige:159586

Publication DOI: 10.1016/j.gloplacha.2022.103784


# A case study of paleoenvironmental interactions during the Miocene Climate Optimum in southwestern Paratethys

Jitka Kopecká, Katarína Holcová, Mihovil Brlek, Filip Scheiner, Lukáš Ackerman, Jan Rejšek, Rastislav Milovský, Viktória Baranyi, Sean Gaynor, Ines Galović, Vlatko Brčić, Mirko Belak, Koraljka Bakrač

PII: S0921-8181(22)00051-0

DOI: https://doi.org/10.1016/j.gloplacha.2022.103784

Reference: GLOBAL 103784

To appear in: *Global and Planetary Change*

Received date: 16 September 2021

Revised date: 31 January 2022

Accepted date: 4 March 2022

Please cite this article as: J. Kopecká, K. Holcová, M. Brlek, et al., A case study of paleoenvironmental interactions during the Miocene Climate Optimum in southwestern Paratethys, *Global and Planetary Change* (2021), https://doi.org/10.1016/j.gloplacha.2022.103784

# A case study of paleoenvironmental interactions during the Miocene Climate Optimum in southwestern Paratethys

Jitka Kopecká[a], Katarína Holcová[b] Mihovil Brlek[c] Filip Scheiner[b/d], Lukáš Ackerman[d], Jan Rejšek[d], Rastislav Milovský[e], Viktória Baranyi[c], Sean Gaynor[f], Ines Galović[c], Vlatko Brčić[c], Mirko Belak[c], Koraljka Bakrač[c]

[a] Department of Biology, Faculty of Education, Palacký University, Purkrabská 2, Olomouc, Czech Republic

[b] Institute of Geology and Paleontology, Faculty of Sciences, Charles University, Albertov 6, 128 43 Praha 2, Czech Republic

[c]Department of Geology, Croatian Geological Survey, Sachsova 2, 10000, Zagreb, Croatia

[d]Institute of Geology of the Czech Academy of Sciences, Rozvojová 269, 165 00, Prague 6, Czech Republic

[e]Earth Science Institute, Slovak Academy of Sciences, Ďumbierska 1, 974 01 Banská Bystrica, Slovakia

[f]Department of Earth Sciences, University of Geneva, Geneva, Switzerland

Keywords: Langhian; foraminifera, calcareous nannoplankton; palynology; Sr-chemostratigraphy; paleoceanological model

**Abstract**

The marine system of the Mediterranean-Paratethys region in the Middle Miocene was influenced by the global climatic changes corresponding to the Miocene Climate Optimum. It was characterized by a global warming of deep oceanic waters succeeded by a decrease of wind activity and ocean water circulation together with a decline in oceanic productivity. This study provides a detailed paleoenvironmental and depositional history of the Middle Miocene deposits from the Mt. Požeška Gora Mountain (the east part of Croatia).. Stable carbon and oxygen isotope data with foraminiferal fauna coupled together with palynological data indicate both seasonal and long-term changes in surface water temperatures, nutrient contents, and salinity. Further, it was possible to determine two

phases of the Middle Miocene flooding in the studied marine system (a) a shallow, high nutrient marginal sea strongly affected by freshwater inputs corresponding to the thermal maximum and periods with enhanced precipitation during the Miocene Climate Optimum; (b) a younger deeper marginal sea with a developed seasonal stratification, rather intermediate nutrient availability and reduced fresh-water inputs. Based on the strontium isotope stratigraphy ($^{87}Sr/^{86}Sr$) coupled with the previously published high-precision geochronology the timing of the first flooding of this marginal sea can be correlated approximately with the Burdigalian/Langhian boundary whereas the second flooding can be correlated to an interval after 15.3 Ma. Possibly, the properties of the surficial waters that were described as a part of the flooding phases in individual time intervals can indicate changes in circulation patterns as a result of potential influence of the Indian Ocean water masses.

## 1. Introduction

The Miocene represents an epoch of major global climatic and paleoceanographic changes such as a well-documented relative warmth during the early to middle Miocene, recorded by benthic oxygen isotope data showing a peak in deep water temperatures at 17.0–14.5 Ma (Zachos et al., 2008), referred as the Miocene Climate Optimum (MCO). General characteristics of the MCO include global warming coupled with elevated temperatures in high-latitude ocean waters, a decline in oceanic productivity, and a marked reduction in the global wind intensity, which resulted in the decreased intensity of surface water circulation and mixing of oceanic water masses (Zachos et al., 2001, 2008; Methner et al., 2020; Sosdian et al., 2020; Brlek et al., 2021; Steinthorsdottir et al., 2021, and references therein). There is considerable evidence that these events were caused by the dissolution of methane hydrates on the oceanic floor, which further led to an abrupt increase of the greenhouse effect in the atmosphere (Wright et al., 1992, Flower and Kennett, 1994, Shevenell et al., 2008, You et al., 2009, Methner et al., 2020 and references therein). In the Paratethys, these climatic and paleoceanographic circulation changes coincided with the local tectonic evolution, resulting in a change in geomorphology which might affect the mesoclimatic conditions. It mainly included the growth of coastal mountain chains that influenced the regional atmospheric circulation, and dramatic

changes regarding the seafloor morphology, which further influenced paleoceanographic circulation patterns. This mesoscale evolution was under the impact of global sea-level and climate changes of that time (Rögl, 1998; Kováč et al., 2007, 2017, 2018; Sant et al., 2017, 2019).

The main aim of this work is to provide a detailed multiproxy reconstruction of the paleoenvironment at the southwestern margin of the Mediterranean-Paratethys marine system with a focus on Central Paratethys (North Croatian Basin; Pavelić, 2001; Pavelić and Kovačić, 2018; Brlek et al., 2020) during the Langhian to assess the impact of the global climatic signal on the large-scale regional evolution, which subsequently influenced the evolution of the whole Mediterranean-Paratethys marine system.

We applied a combination of different methods to be able to assess the complexity of the studied environment; therefore, this study combines rather classical paleontological approaches applied on several key groups of organisms such as calcareous nannoplankton, foraminifera, and dinoflagellate together with a statistical analysis of their quantified records and stable isotope chemistry. To achieve a highly reliable time-constrained model, the age determination was based on chemostratigraphy (strontium isotope stratigraphy, SIS; e.g. Gradstein et al. 2020) and previously published high-precision geochronological constraints (Brlek et al., 2020). Integrated biostratigraphic, chemostratigraphic, and geochronological data provide reliable constraints on the timing of the regional bioevents enabling their comparison to the Mediterranean and the global ones (Kováč et al., 2017, 2018; Sant et al., 2017, 2019; Holcová et al., 2018). Moreover, we discuss the importance of the investigated sections in providing high-quality constraints for the timing of the Middle Miocene transgressions in the North Croatian Basin and on the regional scale (Sant et al., 2017; Kováč et al, 2018; Brlek et al., 2020), as well as for connections of the Central Paratethys with the Mediterranean and the world oceans (Rögl, 1998; Kováč et al., 2017, 2018; Sant et al., 2017, 2019; Holcová et al., 2018; Ivančič et al., 2018).

## 2. Regional settings

The complex system of the epicontinental seas known as the Paratethys stretched since the Early Oligocene (~34 Ma) from the Rhône Basin in France over Central Europe to the Aral Sea in central Asia. The Paratethys was formed by the isolation from the Tethys Ocean and partially communicated with the other successors of the Tethys ocean, the Atlantic Ocean, the Mediterranean Sea, and the Indian Ocean (e.g. Allen and Armstrong 2008; Rögl, 1999; Schulz et al., 2005). From the Oligocene, due to continuous growth of the Alpine–Carpathian–Dinarides orogenic system, the sedimentation space of the Paratehys was gradually isolated, reduced, and divided into the Western, Central and Eastern parts, characterized by different basin configurations and tectonostratigraphic histories (e.g., Rögl, 1998; Popov et al., 2006, Piller et al., 2007, Gozhyk et al., 2015; Neubauer et al., 2015). The Central Paratethys, consisting of epicontinental tectonic basins, was situated in the Alpine–Carpathian–Dinarides orogenic system (Fig. 1A) and represents a large paleogeographic unit covering Central and Eastern Europe from the Oligocene to the Middle Miocene (Rögl, 1998; Popov et al., 2004; Bartol, 2009; Kováč et al., 2017, 2018). The sedimentary record of these basins is an extensive archive of global climate changes superimposed on the local-regional environmental perturbations during the Miocene.

As a result of geodynamic processes, such as the extension of the Pannonian Basin in the Early Miocene and the opening and closure of seaways, the depositional environments of the Central Paratethys basins shifted between open marine to restricted with coastal brackish to lacustrine, as well as alluvial settings. Its sedimentary record reflects changes in tectonics, eustatic, climate, and basin connectivity (Rögl, 1998; Piller et al., 2007; Balázs et al., 2016; Kováč et al., 2017, 2018; Sant et al., 2017, 2019; Holcová et al., 2018). Providing reliable geochronological, chemostratigraphical, and biostratigraphic constraints remains a primary goal to resolve the spatial and temporal evolution of the semi-enclosed Central Paratethys Sea during the Miocene and to correlate the Paratethys strata to the regional and global events (Sant et al., 2017, 2019, 2020; de Leeuw et al., 2018; Kováč et al., 2017, 2018; Brlek et al., 2020).

The North Croatian Basin, comprising the Croatian parts of the Sava and Drava depressions, paleogeographically belongs to the southwestern margins of the Central Paratethys and is located at

the southwestern margin of the Pannonian Basin (Fig. 1A; Pavelić and Kovačić, 2018). It covers almost the entire area of northern Croatia and is situated southeast of the Hrvatsko Zagorje Basin (Fig. 1A), which was a gulf of Trans-Tethyan-Trench-Corridor connecting the Paratethys Sea to the Mediterranean Sea from the Oligocene to the Early Miocene (Rögl, 1998; Mandic et al., 2012; Pavelić and Kovačić, 2018). NCB is an elongated rift-type basin (generated by continental passive rifting) that began forming during the Early Miocene. The syn-rift phase which lasted from the Ottnangian until the Middle Badenian was characterized by depositional environments that changed from continental to marine, with the environments controlled by tectonics, climate, volcanic activity and eustatic fluctuations (Pavelić and Kovačić, 2018). The initial Lower–Middle Miocene (Ottnangian–Lower Badenian *sensu* Pavelić and Kovačić, 2018) sedimentary successions in the North Croatian Basin include continental, alluvial and lacustrine sediments. The initial alluvial deposits (Ottnangian-Karpatian), typically represented by breccias, conglomerates, sandstones and silts with occasionaly intercalated volcaniclastic deposits, were recorded in many places in the North Croatian Basin, including Slavonian Mts. complex (Mt. Psunj, Mt. Papuk and Mt. Požeška gora), where they unconfrmably overlie strongly tectonized and lithologically heterogeneous pre-Neogene basement (HGI, 2009; Pavelić and Kovačić, 2018). Lithologically different continental (salina-type lake) deposits cropping out on Mt. Papuk also suggest strong climatic control on the Early Miocene depositional environments in the North Croatian Basin (Pavelić and Kovačić 2018; Pavelić et al. 2022).The continuation of continental deposition during Middle Miocene (Early Badenian *sensu* Pavelić and Kovačić 2018) is represented by fresh-water lacustrine depositional successions (Southern Pannonian Basin Lake System, SPBLS *sensu* Mandic et al. 2019a)The alluvial–lacustrine series of the North Croatian Basin is generally overlain by Middle Miocene (Badenian) transgressive marine deposits representing widespread ingression(s) of the Paratethys Sea into the North Croatian Basin (Ćorić et al., 2009; Mandic et al., 2012, 2019a; Marković, 2017; Pavelić and Kovačić, 2018; Brlek et al., 2020; Marković et al. 2021).

Mt. Požeška Gora, a part of Slavonian Mts. complex, has recently been the subject of extensive geological investigation, including the finalization of basic geological map 1:50.000 (Fig. 1B; Halamić

et al., 2019), as well as multi-proxy research of Miocene SPBLS and marine deposits with volcaniclastic intercalations (Mandic et al., 2019a; Brlek et al., 2020). All three sections (Tisovac – TIS, Škrabutnik – ŠKR, and Ivan Dol – ID; Figs. 1B, 2) analysed in this work are composed of Middle Miocene (Badenian) Central Parathys marine deposits (13-, 23- and 7-m-thick, respectively) . There are predominant marls, but also clays, silts, sands, and limestones of the Vejalnica Formation (with intercalated volcaniclastic rocks of the Crnka subformation at the ŠKR section) of Middle Miocene (Badenian) age. Marine sediments in the ŠKR section overlie the SPBLS lacustrine marls (Glavnica Formation; Hajek-Tadesse et al. 2009; Ottnangian–Lower Badenian according to Halamić et al. 2019 vs. Lower Badenian according to Kovačić and Pavelić, 2017; Mandic et al., 2019a), although the contact between the Central Paratethyan and SPBLS deposits is not exposed. Similarly, due to lack of contact and the scarcity of outcrops, it is currently not possible to define deposits (e.g., Lower Miocene SPBLS, alluvial or basement) underlying marine sediments (i.e., basal conglomerates) at TIS section (Fig. 2). The contact between basal transgressive Lithothamnium limestones of the ID marine succession and the underlying Glavnica Formation deposits (lacustrine/brackish sediments barren of marine fossils) is of erosional nature (Fig. 2).

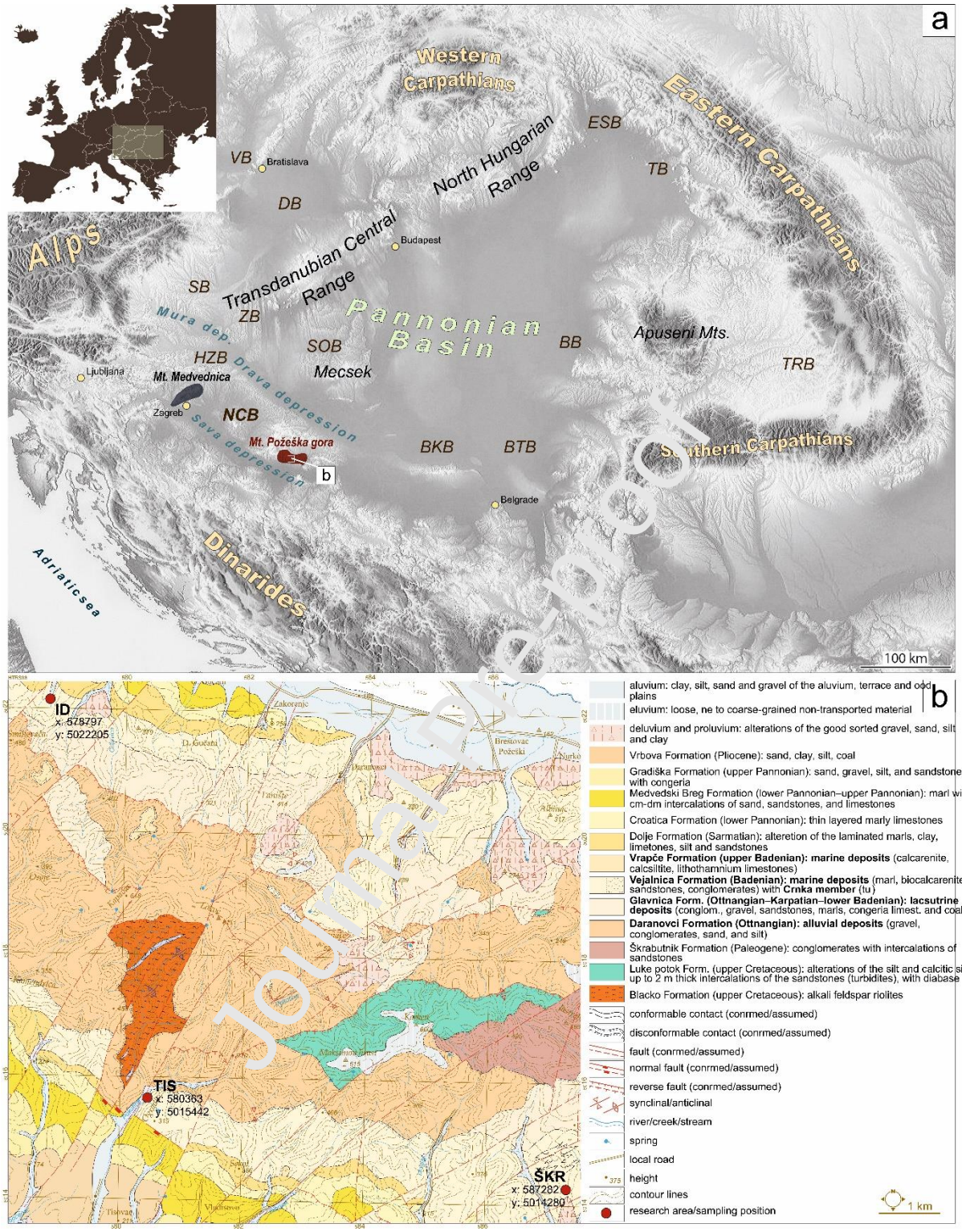


***Figure 1*** *A geographical position of the North Croatian (NORTH CROATIAN BASIN) and other basins of the Carpathian-Pannonian Region (). The position of the Hrvatsko Zagorje Basin (HZB) is also provided. ZB – Zala Basin; SB – Styrian Basin; DB – Danube Basin; VB – Vienna Basin; SOB – Somogy Basin; BKB – Bačka Basin; BTB – Banat Basin; BB – Bèkès Basin; TRB – Transylvanian*

*Basin; TB – Transcarpathian Basin; ESB – East Slovak Basin. B The position of the studied Miocene sections (TIS, ŠKR, and ID) on Mt. Požeška Gora studied here, on part of a modified basic geological map 1:50.000 of Mt. Požeška Gora (Halamić et al. 2019).*

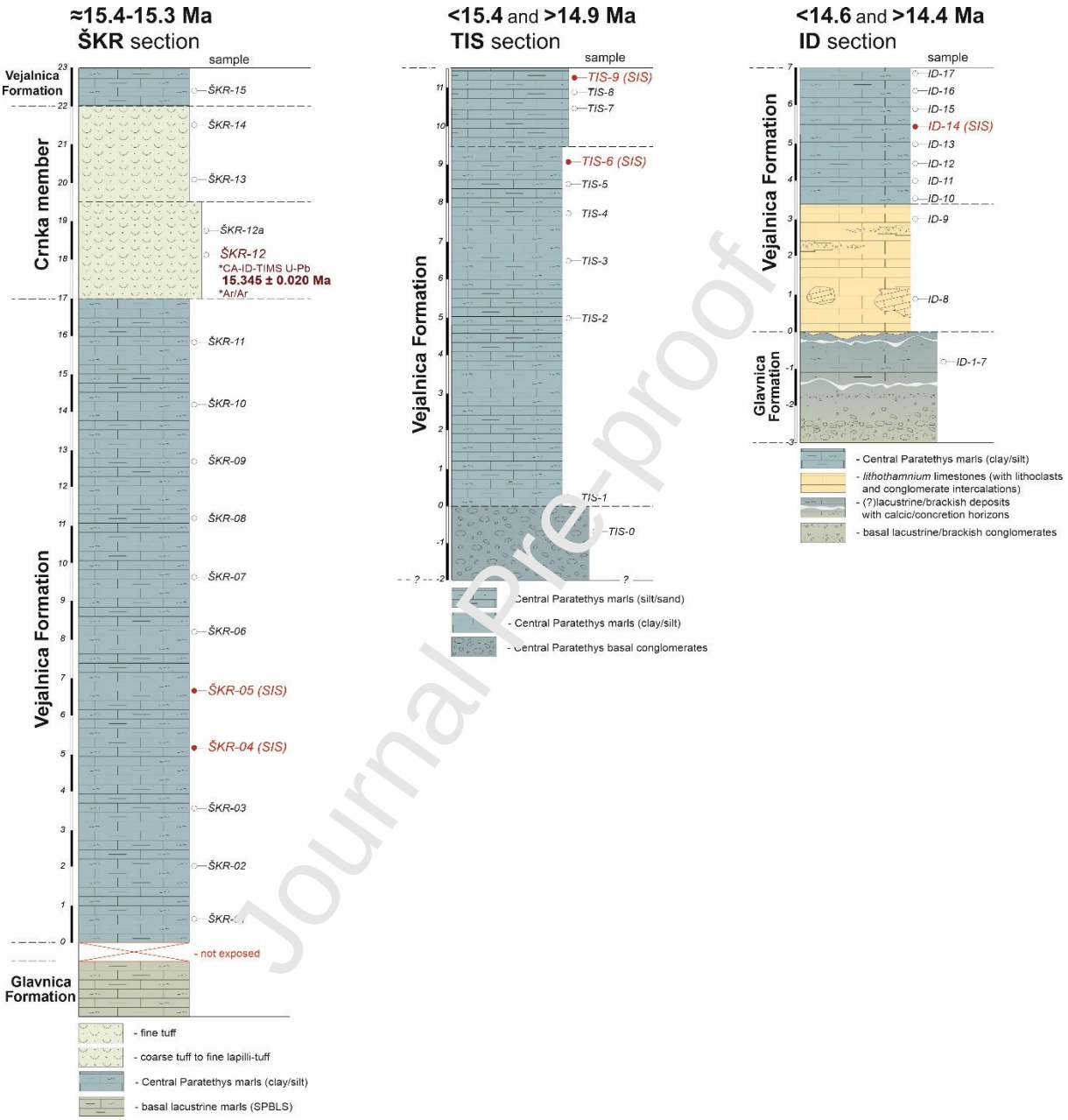


***Figure 2*** *Stratigraphic columns of Tisovac (TIS), Škrabutnik (ŠKR) and Ivan Dol (ID) sections on Mt. Požeška gora, with legend*

## 3. Methods

3.1. Calcareous nannoplankton

Calcareous nannoplankton was studied from smear slides prepared by the method described in Zágoršek et al. (2007) which does not shift the original composition of assemblages. The nannoplankton was counted and determined using an optical microscope, magnification 1000x, parallel and crossed nicols. If possible, around 200—500 specimens per sample were used for quantification of relative abundances of present taxa and further used as the input data for statistical analysis of the present assemblages. For the determination of nannoliths the taxonomical concept followed the one presented in the Nannotax database (Young et al., 2017). The abundance of nannoplankton taxa was expressed as a number of nannoliths in a field of view of a microscope.

3.2 Foraminifera

Foraminiferal assemblages for the paleoecological interpretations were studied from the 0.063–2.0 mm fraction. A total of 4,050 specimens of benthic and planktic foraminifera were picked up and identified in 21 samples from the total number of 38 samples while the rest of the samples were completely barren of microfossils. The foraminifera species were counted and identified using a stereomicroscope Olympus SZX 16, and for the precise determination of small planktic species a scanning electron microscope at the Department of Geology, Palacký University, Olomouc, Czech Republic was used. The statistical program *PAST* (Hammer et al., 2001) was used for the statistical analyses of the foraminiferal assemblages. Foraminiferal species for the single-shell oxygen and carbon stable isotopic analysis were picked up of approximately the same size to minimize any ontogenetic effects. The preservation state of the material was evaluated under the SEM based on the character of the inner-wall structure. With respect to this evaluation, we further selected samples that had no indications of any diagenetic alteration for the subsequent stable isotopic analyses. The selected taxa were chosen based on their variable ecological preferences to document both, the water column and sea-floor environments.

3.3 Palynology

Fifteen samples from the Škrabutnik and Tisovac sections have been selected for subsequent palynological analysis. The organic particles were extracted applying standard procedures after e.g.

Moore et al. (1991) and Wood et al. (1996) that included crushing of *ca*. 37 g of sediment and disintegrating it with sodium pyrophosphate ($Na_4P_2O_7$), followed by an acid treatment. At the beginning of the procedure, the samples were spiked with two *Lycopodium* tablets (9666 *Lycopodium*/tablet) to dissolve the carbonate and silicate fraction, the sediment was treated with cold HCl (15%) and HF (40%). Heavy liquid separation with $ZnCl_2$ (density >2.1 kg/l) was used to separate the organic matter from the remaining undissolved inorganic components and the organic residue was sieved through a 10 µm mesh while the palynological slides were mounted in glycerine. Microscopic analyses were performed using an Olympus BH-2 at 200x and 400x magnification. Photomicrographs were taken with an AmScopeTM camera adapter connected to the AmScope v.3.7 software. Since the samples yielded very little organic matter, the entire residue was used for preparing palynological slides and all slides were scanned subsequently. All encountered palynomorphs were counted. The slides are housed at the Department of Geology, Croatian Geological Survey.

3.4 Stable carbon and oxygen isotopes

Stable isotope analyses of foraminifera were performed on a mass spectrometer MAT 253 coupled to an automated preparation device Kiel IV via the dual-inlet interface. Individual or pooled foraminiferal shells weighing typically between 20–30 micrograms were loaded into borosilicate vials and reacted with anhydrous phosphoric acid at 70°C in a vacuum following the method of McCrea (1959). After the cryogenic removal of permanent gases and hydrocarbons, the purified $CO_2$ was measured for the stable C and O isotopes. Values are reported as per mille vs. VPDB (Vienna Pee Dee Belemnite) and they were calibrated using cylinder $CO_2$ gas with known composition, traceable to the international reference material NBS18 with $\delta^{13}C$ = +5.014 ‰, $\delta^{18}O$ = –23.2 ‰. Each batch of 21 samples was bracketed by 3 samples of a working standard Mab3 with $\delta^{13}C$ = +2.48 ‰, $\delta^{18}O$ = –2.40 ‰ to verify the accuracy of the measurement. The typical internal precision of the measurement is 0.04 ‰ for carbon and 0.06 ‰ for oxygen. Linearity of delta values against the signal intensity was tested on 60 measurements of a working standard of variable weights typical for studied foraminifera, upon which correction equations were regressed for $\delta^{13}C$ and $\delta^{18}O$ vs. mass 44 and mass 46 amplitude, respectively. The correction has a form of the three-parameter logistic equation:

$$\delta^{13}C_{CORR} = \delta^{13}C_{MEAS} + 0.1666 - 0.3803 * (1 - e^{-0.0051 * AMP}) \quad \text{eq. 1}$$

$$\delta^{18}O_{CORR} = \delta^{18}O_{MEAS} + 0.23 - 0.727 * (1 - e^{-0.0053 * AMP}) \quad \text{eq. 2}$$

where $\delta^{13}C_{CORR}$ and $\delta^{18}O_{CORR}$ are corrected value, $\delta^{13}C_{MEAS}$ and $\delta^{18}O_{MEAS}$ are measured values, AMP is the amplitude of mass 44 ($^{12}C-^{16}O-^{16}O$) in millivolts. The $R^2$ values of the regressions are 0.9448 and 0.9787 for carbon and oxygen, respectively.

3.5. $^{87}Sr/^{86}Sr$ values

Only well-preserved foraminifera, otholiths, molluscs and ostracods were picked for Sr isotope analysis. The preservation was checked under an SEM and the influence of fresh-water input in the studied marine ecosystem was evaluated based on the stable oxygen isotope data (McArthur et al., 2001, Gradstein and Ogg, 2020 and references therein).

The Microfossils were processed at the clean lab of the Institute of Geology of the Czech Academy of Sciences (IG CAS). The samples were crushed and then treated using ultrapure water (Millipore Element), alkali-buffered 1 % $H_2O_2$ solution, and weak $HNO_3$ to remove possible clay particles, organic matter, coarse-grained silicate and other contaminations (Barker et al., 2003). Afterward, the samples were quickly (30 seconds) leached using 0.001 M $HNO_3$ and finally dissolved in 1 M $HNO_3$ and processed for Sr separation. Strontium was isolated from the matrix by ion-exchange chromatography using Sr resin (Triskem, France) with 2 ml of 0.05 M $HNO_3$ used for Sr collection (Pin et al., 2014). The solution was dried and loaded in 6 M HCl onto degassed Re filaments in the presence of Ta activator and $^{87}Sr/^{86}Sr$ determination was performed on a Thermo Triton Plus thermal ionization mass spectrometer (TIMS) housed at the IG CAS using Faraday cups employed in a static mode and $^{88}Sr/^{86}Sr$ of 8.3752 for mass fractionation correction. External reproducibility of the measurements was accessed through the periodical analyses of the NIST SRM 987 solution that yielded $^{87}Sr/^{86}Sr$ of 0.710239 ± 0.000008 (2σ, n = 20).

$^{87}Sr/^{86}Sr$ values were converted into numerical ages using the regression curve LOWESS look-up Table version 6 (McArthur et al. 2020). Minimum and maximum ages were obtained by combining the

statistical uncertainty (2σ) of the mean values of the Sr-isotope ratios of the samples with the uncertainty of the seawater curve.

## 4. Results

### 4.1. Calcareous nannoplankton

Calcareous nannoplankton was identified in 21 samples from a total of 38 analysed samples. It is very rare to rare in the sections TIS and ŠKR and common to very abundant in the upper part of the ID section (Fig. 3A). *Coccolihus pelagicus*, *Reticulofenestra minuta* and helicospheras (*H. carteri*, *H. walberdorfensis* together with less numerous *H. waltrans*, *H. amoliapperta*) dominate in the studied assemblages (Figure. 3B, C; Appendix 1). Reworked taxa are generally very rare to rare (to 5%) and they are of the Cretaceous and Oligocene ages. The only exception represents Cretaceous redeposits in the interval ŠKR 7–9 m where the reworked taxa reached values between 5–15% (Figue 3D; Appendix 1).

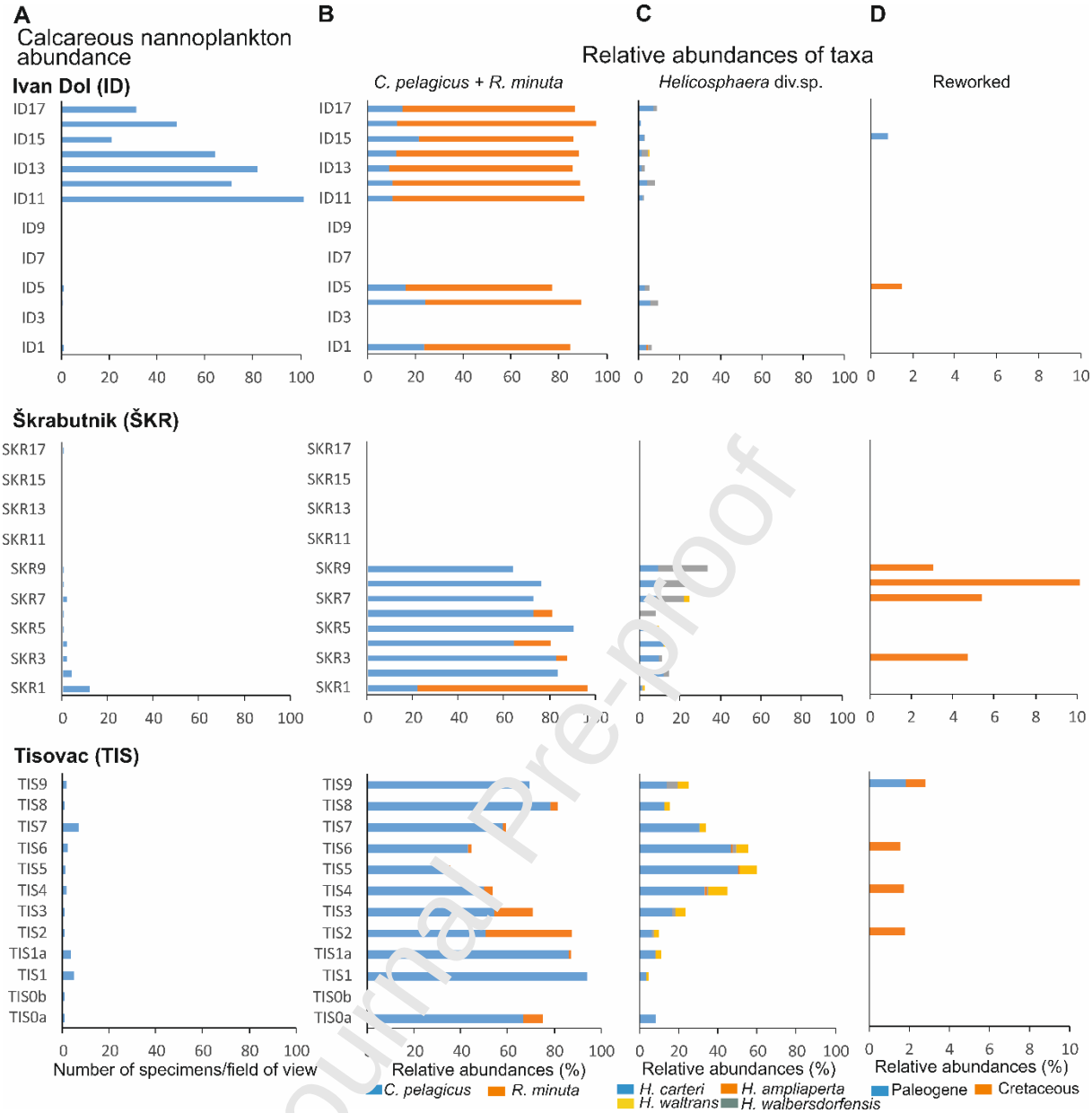


***Figure 3*** *Quantitative characteristics of the calcareous nannoplankton assemblages. A-Abundance expressed as a number of specimens/a field of view of microscope averages for 50 fields of view; B-C Relative abundances of the most common taxa (B-Coccolithus pelagicus and Reticulofenestra minuta, C-helicosphaeras); D-relative abundances of reworked taxa.*

The statistical analysis (Principal Component Analysis - PCA) gave statistically significant results for two coordinates which represent 96.9 % of the variance (Table 1). Three calcareous nannoplankton assemblages can be distinguished using this method (Figure 4A): (1) the *Coccolithus pelagicus* assemblage containing more than 50 % of the nominate taxon; (2) the *Helicosphaera* assemblage reaching more than 30 % of large *Helicosphaera* div. sp., mainly *H. carteri*. The relative abundances

of large helicosphaeras positively correlate with *Coccolithus pelagicus* (Table 2), and the assemblages (1) and (2) partly overlap; (3) the *Reticulofenestra minuta* assemblage differs from the assemblages (1) and (2), and it is significantly dominated by the nominate species representing more than 60 % of the assemblages.

**Table 1** *The percentage of variance for individual coordinates of the PCA classification of the calcareous nannoplankton assemblages*

| PC | Eigenvalue | % variance |
|---|---|---|
| 1 | 1872.95 | 86.215 |
| 2 | 227.499 | 10.472 |
| 3 | 38.3468 | 1.7652 |
| 4 | 18.5743 | 0.855 |
| 5 | 5.48597 | 0.25253 |

***Table 2*** *Statistically significant (pvalue <0.001) Spearman correlation coefficients (yellowed) between the relative abundances of calcareous nannoplankton taxa in the studied assemblages.*

| | *Coccolithus pelagicus* | *Helicosphaera carteri* | *Reticulofenestra minuta* |
|---|---|---|---|
| *Reticulofenestra haqii* | -0.30 | 0.47 | 0.61 |
| *Helicosphaera waltrans* | 0.71 | 0.57 | -0.32 |
| *Helicosphaera carteri* | 0.67 | 0.00 | -0.05 |

For the detailed distribution of the assemblages along the studied sections see Figure 4B. The *Coccolites pelagicus* assemblages dominate in the lower part of the TIS section (TIS1–4) and in the ŠKR section. This assemblage is substituted by the *Helicosphaera* one in the upper part of the TIS section. The *Reticulofenestra minuta* assemblages characterize the ID section.

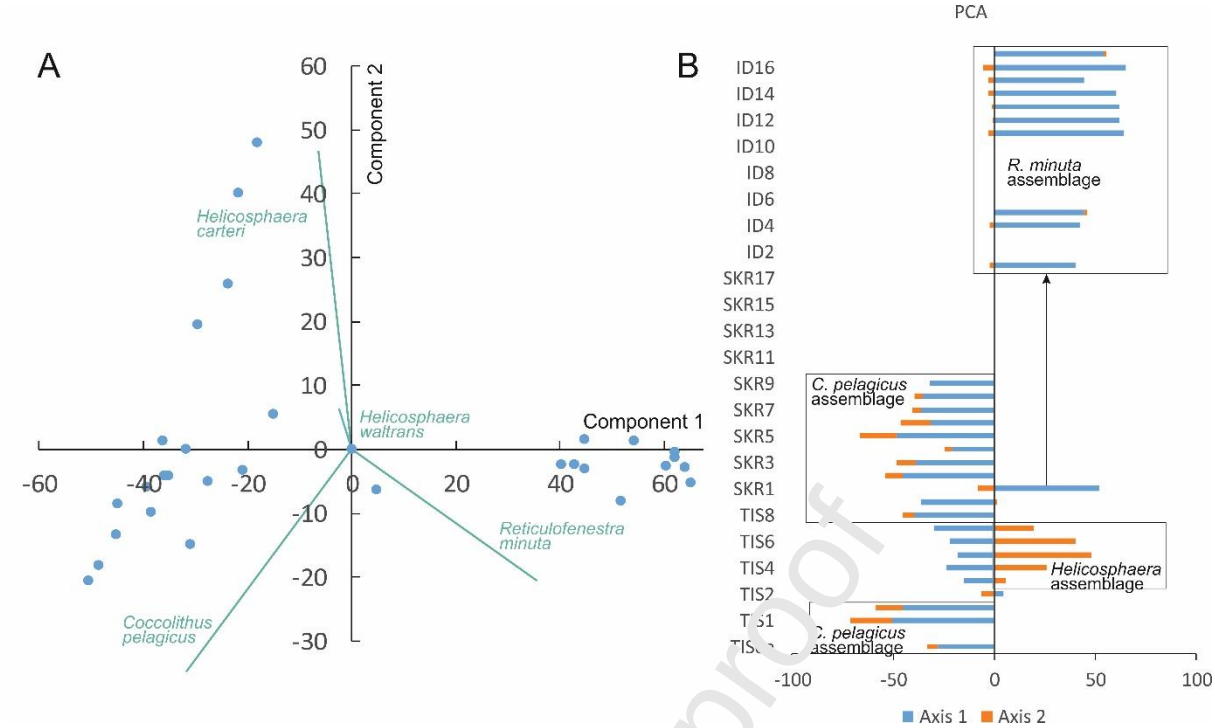


**Figure 4** *The classification of calcareous nannoplankton assemblages using the principal component analysis. A Biplot (scatters and loadings values for the components 1 and 2), Scatter values for individual samples showing the distribution of statistically defined assemblages along the sections*

4.2. Foraminifera

Foraminiferal assemblages are characterized by a high plankton ratio. In a majority of the evaluated samples, the value reached more than 60 %. In the intervals of the TIS 1–TIS 5, ŠKR2, ŠKR3, ŠKR8 and ŠKR9 there were even more than 80 % of planktic species; nevertheless, the assemblages of planktic foraminifera are characterized by a generally low diversity. The values of the Shannon–Wiener index range between 1.02 (TIS 7) and 2.34 (ID 11) with a median of 1.96. The low values of diversity correlate well with the high values of the dominance index, which ranges from 0.11 (ŠKR 4) to 0.42 (TIS 7) with a median of 0.17 (see Figure 5A).

Planktonic small "four-chambered" (*Globigerina falconensis, Globigerina praebulloides/bulloides, Globigerina connecta)* and "five-chambered" globigerinids (*Globigerina bollii, Globigerina tarchanensis*); *Globigerinita* groups, *Tenuitella* groups, *Tenuitellinata selleyi*, and *Turborotalia quinqueloba* are the most important planktic fauna with a high dominance between 53 to 100 % in the

planktic assemblages. The species *Turborotalia quinqueloba, Globigerina tarchanensis, Globigerina bulloides/praebulloides, Tenuitellinata selleyi, and Tenuitella* prevailed at the ŠKR and TIS sections; *Orbulina-Praeorbulina, Globorotalia,* and *Globigerinoides* groups reached high abundance in the ID sections together with *Globigerina praebulloides*. Ocasionally also *Paragloborotalia mayerii* dominated (ŠKR 15 and ID 17 samples).

Species *Globigerina praebulloides/bulloides, Globigerina tarchanensis, Turborotalia quinqueloba, Tenuitellinata selleyi* and *Tenuitella clemenciae* are significant for interpretation of rich nutrient environment, species of *Globorotalia/Paragloborotalia ,Globigerinoides* and *Orbulina-Praeorbulina* groups are important for warm surface water interparetation. For the distribution of these paleoecological markers through the sections see Figure 5B and Appendix 2.

Benthic foraminiferal assemblages resemble the planktic assemblages by low values of diversity and abundance indices (Figure 5A). The benthos ratio > 50 % was calculated only for the assemblages from the ID section (comparison with the plankton ratio in Figure 5A, Appendix 2). At the TIS and ŠKR sections, there is a significant presence of the *Bolivina – Bulimina –Causassina* group together with the *Cibicidoides – Elphidium* group (see Fig. 7 A,B, Appendix 2), uniserial foraminifera with the dominant *Heterolepa* group at the ŠKR sections and the *Laevidentalina – Siphonodosaria* group at the ID sections (see Figure 7 D, Appendix 2). For the paleoecological interpretation, there is significant occurrence of *Bolivina hebes* and *Caucasina subulata* as low oxygen indicators, *Pullenia bulloides, P. quadriloba, Hansenisca soldanii, Melonis pompilioides* and *Valvulineria complanata* for interpretation of high nutrient environment, *Heterolepa* group together with uniserial groups for food availability interpretation and *Cibicidoides* sp. And *Elphidium* sp. for oxic condition interpretation. The distribution of these markers is illustrated in Figure 5B and Appendix 2.

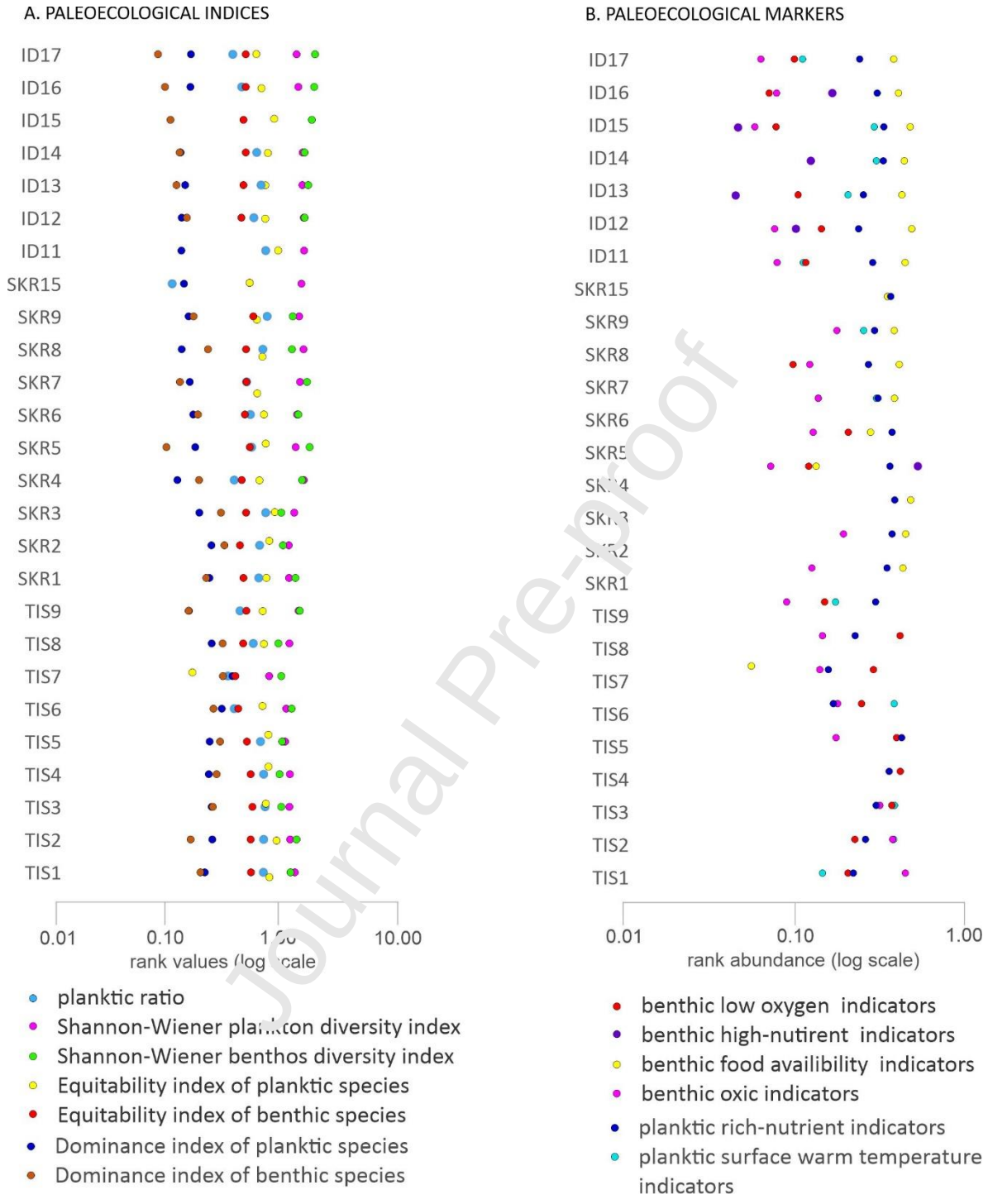


***Figure* 5** *Rank of significant foraminiferal paleoecological indices and markers*

The statistical analysis of foraminiferal assemblages using the PCA method was carried out separately for planktic and benthic species (Figure 8; 9). The analysis of planktic foraminifera reached for two coordinates 69 % of the variance; for three coordinates 82.6 % (Table 2).

***Table 3*** *The percentage of variance for individual coordinates of the PCA classification of the planktic foraminifera assemblages*

| PC | Eigenvalue | % variance |
|---|---|---|
| 1 | 505.078 | 41.544 |
| 2 | 334.27 | 27.494 |
| 3 | 164.584 | 13.537 |

Three statistically defined assemblages can be correlated with the individual sections: (1) the *G. tarchanensis – T. quinqueloba* assemblages characterize the TIS section. In the upper part of the section, the abundances of *G. uvula* increase (Figure 6) similarly to the assemblages from the ŠKR section. This increase coincides with the distribution of the *Helicosphaera* assemblage of calcareous nannoplankton (Figure 4). (2) The *Tenuitella – G. uvula* assemblage was recorded in the ŠKR section. (3) The *Globigerinoides trilobus Globigerina praebulloides* assemblage was recorded in the ID section. This assemblage differs primarily by the presence of larger planktic foraminifera.

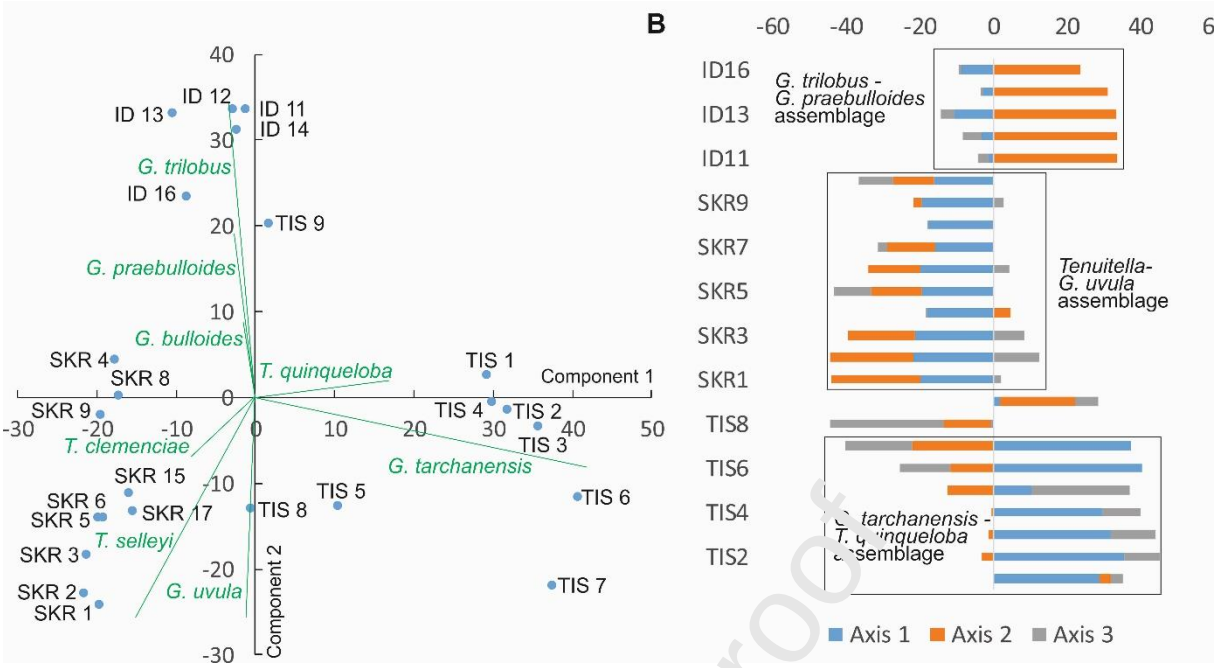


***Figure 6*** *Classification of planktic foraminifera assemblages using the PCA. A Biplot (scatters and loadings values) for components 1 and 2); B Scatter values for the individual samples showing the distribution of the statistically defined assemblages along the sections*

The benthic foraminifera were classified into three distinct assemblages, which correspond well with the individual studied sections (Figure 7). Three coordinates represent 85.8 % of the variance (Table 4). The TIS section matches with: (1) the *Bolivina hebes-Valvulineria-Cibicidoides* assemblage, but *Valvulineria* occurs commonly only in the less-diversified assemblages in the upper part of the section together with the increased presence of large helicosphaeras and *G. uvula;* (2) The *Heterolepa-Fonbothia* assemblage was recorded in the ŠKR section except the sample ŠKR4 related to (3) the monoserial lagenids-*Lenticulina-Pullenia* assemblage occurring also in the ID section (Figure 9)

***Table 4*** *The percentage of variance for individual coordinates of the PCA classification of the benthic foraminiferal assemblages*

| PC | Eigenvalue | % variance |
|---|---|---|
| 1 | 1037.42 | 54.14 |
| 2 | 314.195 | 16.397 |
| 3 | 293.295 | 15.306 |

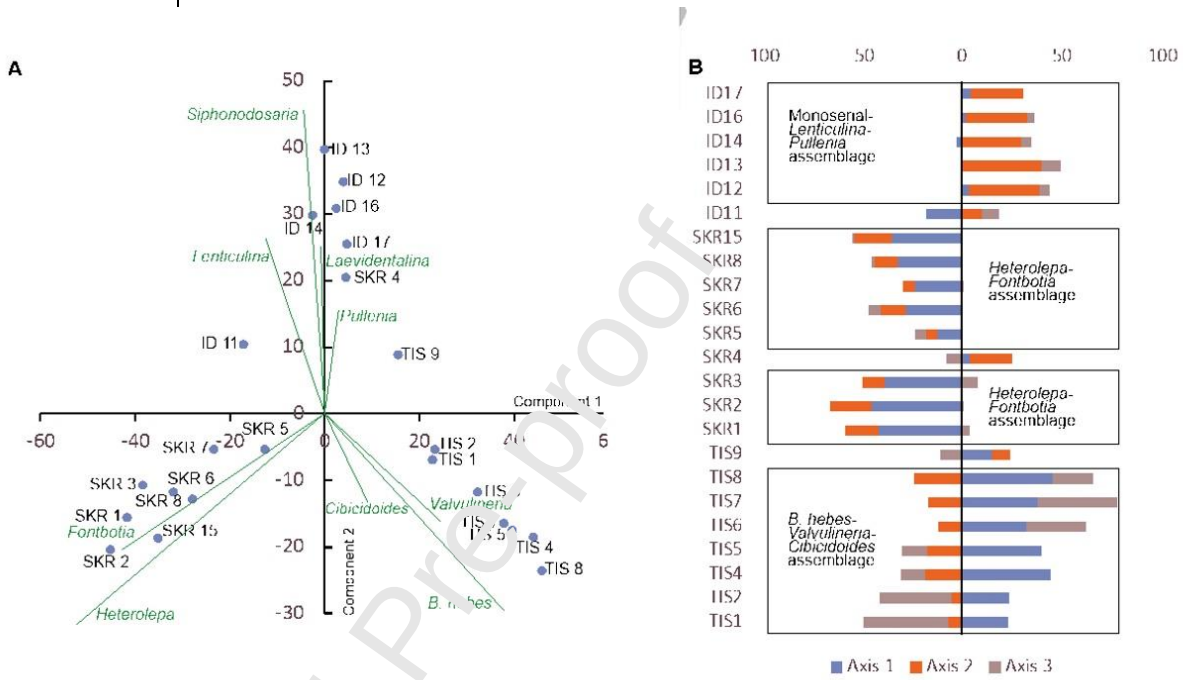


***Figure 7*** *Classification of benthic foraminiferal assemblages using the PCA. A Biplot (scaters and loadings values) for components 1 and 2); B Scatter values for individual samples showing the distribution of statistically defined assemblages along the sections*

4.3. Palynology

The palynological samples from the TIS and ŠKR sections yielded a moderate amount of sedimentary organic matter and the preservation of the palynomorphs was poor to moderate. Their abundance is very variable ranging from <50 counts in the samples from the ŠKR section to >500 in the TIS section. Aquatic palynomorphs were identified only in samples ŠKR 1, 4, 7, and 8. Dinoflagellate cyst assemblages from the ŠKR section are highly impoverished with only five identified species present and with a maximum abundance of 19 counts in sample ŠKR 1. The section TIS reveals a moderately

preserved and moderately diverse dinoflagellate cyst assemblage. The highest diversity and abundance were recorded in the sample TIS 4 with a total abundance of 210 dinoflagellate cyst belonging to 19 different species. The abundance is much lower in the remaining samples (<50 counts), while the basal conglomeratic layers (TIS 0) contain a very low number of palynomorphs. The most common dinoflagellate cyst species from the TIS and ŠKR sections are: *Cleistoshaeridium placacanthum, Polysphaeridium zoharyi, Spiniferites ramosus, S. pseudofurcatus, Operculodinium* sp., and *Lingulodinium machaerophorum*. A single specimen of *Impagidinium* sp. was recorded in the TIS 4 sample. *Cribroperidinium tenuitabulatum* is also present in the same sample (TIS 4). The cavity cyst, *Cousteaudinium aubryae* is persistently recorded in the TIS section, and its abundance slightly increases upsection. Peridinoid cysts (*Lejeunecysta* spp, *Selenopemphix* sp., *Sumatradinium* spp.) are common in the TIS 2 and 4 samples, but they are absent from the top of the section. Despite the moderate abundance and diversity of dinocysts at the TIS section, the palynological samples are dominated by bisaccate pollen grains ranging from 87 % to 100 % of the total palynological counts. They include pollen of *Pinus, Cathaya,* and some indeterminate pollen of the Pinaceae group. Pollens of the Taxodioideae are present, although they are rare. Angiosperm pollen (*Tilia*, *Ulmus*, *Carya*) and spores (*Polypodium*, *Polypodiaceoisporites* sp.) contribute to the terrestrial fraction to a much smaller extent and are usually represented by <10 counts each. Freshwater algae (*Pediastrum, Botryococcus braunii*) are extremely rare in both sections. The palynofacies of this TIS and ŠKR section consist mainly of terrestrially derived phytoclast particles with distinct internal structures e.g., pits, rays, consistent with an origin from a higher vascular plant, and degraded brown-black wood particles without discernible biostructure. Cuticle particles are scarce.

4.4. Geochemistry

The $\delta^{18}O$ values in the TIS samples for small globigerinids-*Globigerina tarchanensis*/*falconensis* range from –6.7 ‰ to –2.5 ‰ with the $\delta^{13}C$ range between –1.4 ‰ to –1.2 ‰. Benthic species are represented by *Cibicidoides ungerianus* with the $\delta^{18}O$ values ranging from –3.4 ‰ to –1.5 ‰ with the $\delta^{13}C$ range from +0.4 ‰ to +1.6 ‰.

In the ŠKR samples the $\delta^{18}O$ values for *Globigerina bulloides/praebulloides* range from –1.8 ‰ to +0.8‰ while $\delta^{13}C$ range from –0.1 ‰ to +0.8 ‰. Small globigerinids-*Globigerina tarchanensis/falconensis* $\delta^{18}O$ values range between –4.9 ‰ to –3.2 ‰. The $\delta^{13}C$ values range from –1.7 ‰ to –1.1 ‰. Amongst the benthic species the $\delta^{18}O$ values for *Cibicidoides ungerianus* exhibit a broad range from –3.3 ‰ to –0.3 ‰ while $\delta^{13}C$ range from –0.9 ‰ to +0.7 ‰. The *Melonis pompilioides* $\delta^{18}O$ ranges from –2.4 ‰ to –0.9 ‰ with the $\delta^{13}C$ ranging between –1 ‰ to –0.5 ‰. The $\delta^{18}O$ values for *Pullenia bulloides* range from –2.6 ‰ to –0.4 ‰ while $\delta^{13}C$ values range is –1.1 ‰ to –0.1 ‰.

In the sample ID14 the $\delta^{18}O$ for *Globigerinoides trilobatus* range between – ‰ to –1.4 ‰. The $\delta^{13}C$ is within a range from +2.1 ‰ to +3.1 ‰. In the sample ID 16, the *Globigerina bulloides/praebulloides* $\delta^{18}O$ ranges from –2.7 ‰ to –0.5 ‰ with the $\delta^{13}C$ value spreading from –0.8 ‰ to +0.8 ‰. Regarding the benthic species the $\delta^{18}O$ values of *Cibicidoides ungerianus* range from –2.6 ‰ to –0.3 ‰ while the $\delta^{13}C$ ranges between –0.6 ‰ to +1.4 ‰. Finally, the *Melonis pompilioides* $\delta^{18}O$ values range from –2.6 ‰ to +0.3 ‰. The $\delta^{13}C$ values spread from –0.7 ‰ to +0.6 ‰ forming the main cluster between –0.7 ‰ to +0.1 ‰ (see Figure 8).

Normal distribution of the data was tested using the PAST software (Hammer et al., 2001). For the complete data, see Appendix 1.

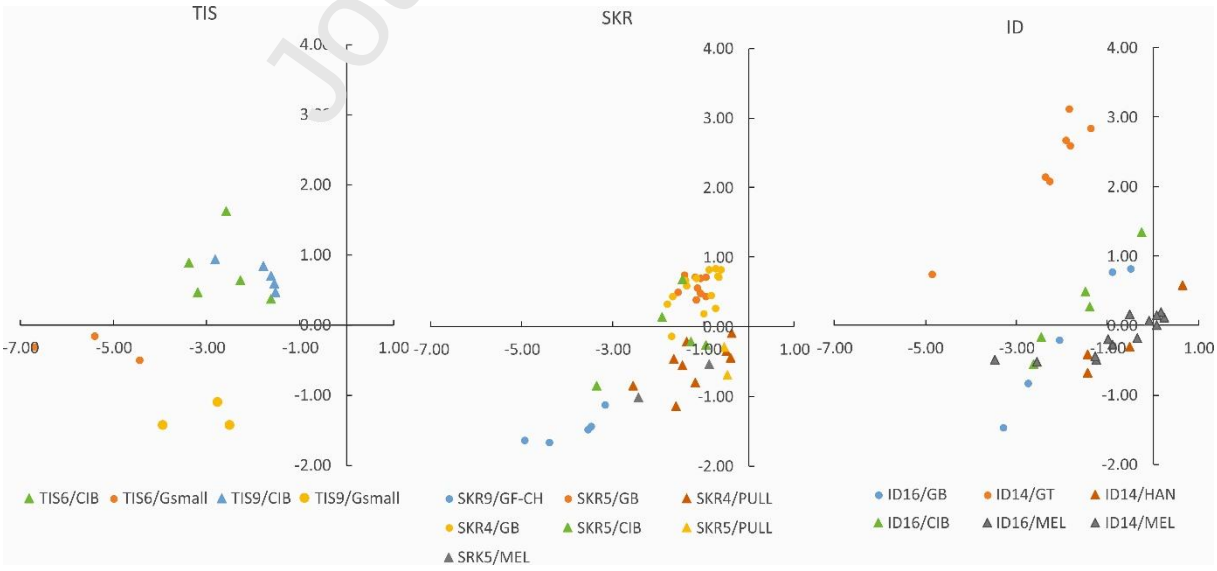

***Figure 8*** The oxygen and carbon isotope data. CIB – *Cibicidoides ungerianus*, GB – *Globigerina bulloides*, Gsmall – small *Globigerina tarchanensis*, GT – *Globigerinoides trilobatus*, *GF-CH Globigerina falconensis*, *PULL – Pullenia bulloides*, *MEL – Melonis pompiloides*, *HAN – Hansenisca soldanii*

The isotopic ranges are in agreement with the presumed habitats of the selected foraminiferal species. Moreover, Scheiner et al. (2018) show a range of intra-species isotopic variability in a similar epicontinental environment using the single-test approach, which was also used in this study. Considering our isotopic data, the inter-species variability is definitely present, see Figure 8. Based on the conditions of the studied environment then our isotopic data represents primarily a combination of several factors. Besides the evolution of the global signal, isotopic data are influenced also by the so-called vital effects, especially the benthic species (e.g. Schmiedl et al., 2004), but we believe the main component is closely related to the primary environmental parameters such as the temperature, salinity and nutrient availability.

## 5. Interpretation and discussion

### 5.1. Age model

The presented age model is primarily based on microbiostratigraphy and it had been confronted with the previously published radiometric ages (Brlek et al., 2020) for its confirmation. The following micro- and nanno-biostratigraphic index taxa were recorded in the studied sections: *Helicosphaera ampliaperta* (a continuous occurrence in the samples TIS 4–6; an isolated occurrence in the ID 1 sample), *H. waltrans* (a continuous occurrence in the TIS section; an episodic occurrence in the ŠKR section; an isolated presence in the sample ID 14), *Praeorbulina circularis* (FO in the sample ID 11) and *Orbulina* (FO in ID 12; Figure 9 B). The numerical ages estimated for these events for the Mediterranean area as well as for the world oceans (Figure 9A; di Stefano et al., 2008; Aziz et al., 2008; Iaccarino et al. 2011; Turco et al. 2017; Gradstein and Ogg, 2020; Young et al., 2021) were confronted with the previously published radiometric ages by Brlek et al. (2020). The first continual

occurrence of *Helicosphaera waltrans* is dated at 15.47 Ma in the Mediterranean area by Iaccarino et al. (2011) and later this was revised to 15.4 Ma by Turco et al. (2017). It indicates that the TIS section should be younger than 15.4 Ma. On the other hand, the occurrence of *Helicosphaera ampliaperta* suggests an older age than the LO of this taxa, i.e. 14.9 Ma (Gradstein and Ogg, 2020; Young et al., 2021). From a biostratigraphic point of view, the sedimentation of the TIS section can be dated within the time interval consisting of the lower boundary being <15.4 Ma and the upper boundary >14.9 Ma. Nevertheless, the exact time determination within this interval is unable in this case.

*Helicosphaera waltrans* is the only index taxa that was recorded in the ŠKR section. The occurrence of this taxa indicates that the section have to be younger than 15.4 Ma. The radiometric datums from the upper part of the ŠKR section (ŠKR-12 coarse tuff to fine lapilli tuff), provided the CA-ID-TIMS U–Pb zircon age 15.345 ± 0.020 Ma as well as the Ar/Ar sanidine ages 15.34 ± 0.32 Ma and 15.43 ± 0.32 Ma (Brlek et al., 2020). This indicates that the sedimentation of the lower fossiliferous part of this section started immediately after the first occurrence of the *Helicosphaera waltrans* (~ 15.4 Ma).

The age of the ID section can be biostratigraphically interpreted only in the upper, fully marine part. A sole specimen of *Helicosphaera ampliaperta* recorded at the base of the ID section is representing probably reworked taxawith respect to the lacustrine/brackish origin of this strata. The suggested non-marine origin of the lower part of this section is also supported by the absence of foraminifera. The nearly simultaneous appearance of *Praeorbulina circularis* and *Orbulina suturalis* in the upper part of the ID section agrees well with the analogous situation in the other Central Paratethyan basins (Holcová et al., 2018). If we use the Mediterranean dating of these bioevents (14.9 Ma for the FO of *Praeorbulina circularis* and 14.6 Ma for *Orbulina suturalis*; Abdul Aziz et al. 2008), it implies that the upper part of the ID section has to be younger than 14.6 Ma. The occurrence of *Helicosphaera waltrans* in the sample ID 14 indicate age >14.4 Ma (= LO of *Helicosphaera waltrans*; Abdul Aziz et al. 2008) in case that the specimens are autochthonous.

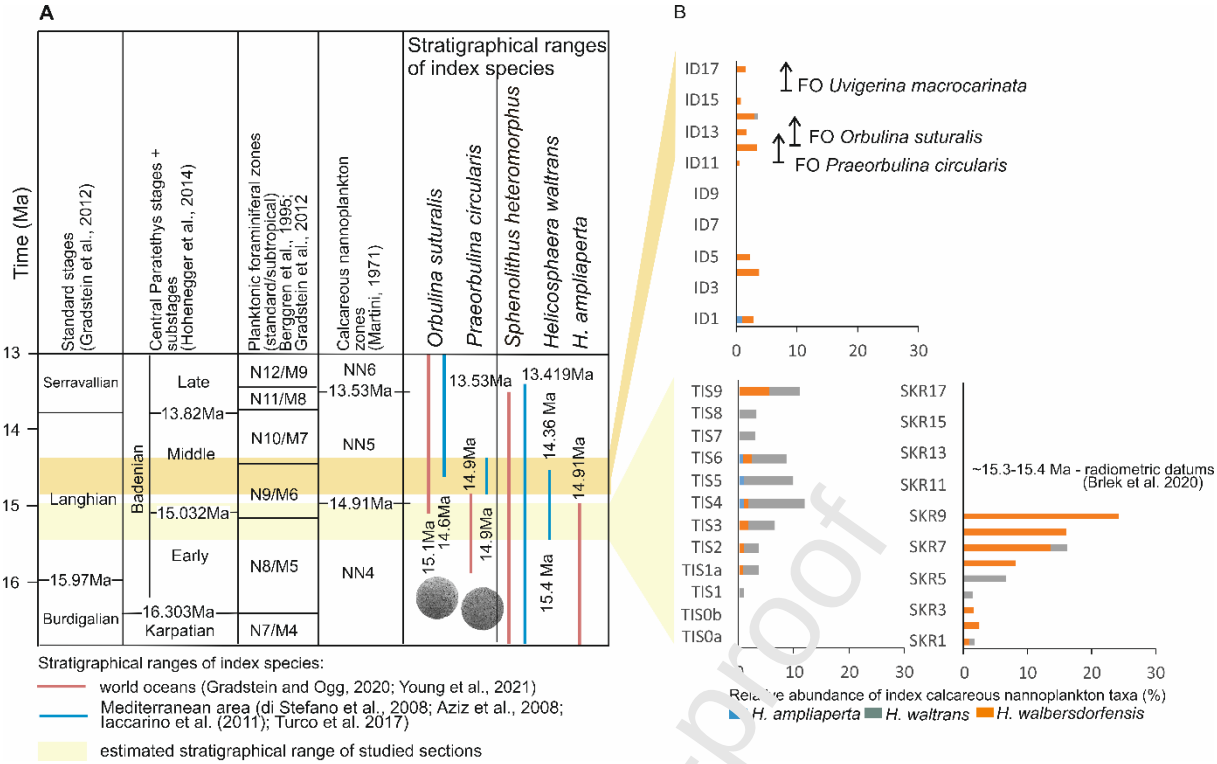


***Figure* 9** Quantitative biostratigraphic data for the studied sections. A synthesis of biostratigraphic datums from literature; B Calcareous nannoplankton and foraminifera\ biostratigraphic markers

The dinocyst biostratigraphy corroborates the above-mentioned results. The persistently recorded occurrence of *Cousteaudinium aubryae* in the TIS section is correlated to the late Burdigalian-early Langhian and the upper part of the NN4 nannoplankton zone in the Mediterranian region (Zevenboom, 1995). The highest occurrence of *Cousteaudinium aubryae* is calibrated against the base of the C5Bnln chron at ca. 14.9 Ma in the early Langhian in Northern Hemisphere mid-latitudes (Zevenboom, 1995; Munsterman and Brinkhuis, 2004; Williams et al., 2004), which does not conflict with our results. In Croatia, *C. aubryae* is present until the top of the *Cribroperidinium tenuitabulatum Zone* (Cte) that is of Langhian age (Bakrač et al., 2012). *Cribroperidinium tenuitabulatum* recorded only in TIS 4 delimits the upper boundary of the *Cribroperidinium tenuitabulatum* Assemblage Zone (*Cte Zone*) that is in Croatia calibrated against the NN4–NN5 calcareous nannoplankton Zones (Bakrač et al., 2012). The dinoflagellate cyst-based biostratigraphical range top of the studied interval is constrained by the occurrence of *Unipontidinium aquaeductus* from the upper part of the Ivandol section (unpublished data, Baranyi and Bakrač, 2020). In the world ocean the lowest occurrence of *U. aquaeductus* is

correlated with nannofossil zone NN5 in well-constrained sections from the eastern USA (de Verteuil & Norris, 1996), northern Germany (Strauss et al., 2001), and Belgium (Louwye et al., 2000). Although, the base of NN5 is somewhat debated (see discussion in Jiménez-Moreno et al., 2006), currently it is placed at 14.897 Ma in the world ocean (Bergen et al., 2019). Thus, the lowest occurrence of *U. aquaeductus* from the Central Paratethys realm can be also considered to be mid-Langhian within the interval of 15.1–14.8 Ma (Jiménez-Moreno et al., 2006) suggesting that the upper part of the Ivandol section is younger than that.

The above mentioned biostratigraphic and radiometric datums are not fully comparable with chemostratigraphy (SIS = strontium isotope stratigraphy; Table 5) what is suggested by the local $^{87}Sr/^{86}Sr$ signal. The comparison of the measured $^{87}Sr/^{86}Sr$ values using the regression curve LOWESS look-up Table version 6 (McArthur et al. 2020) showed that the measured $^{87}Sr/^{86}Sr$ values are lower than the expected ones , (Fig. 12A).

| Sample | Analysed material | $^{87}Sr/^{86}Sr$ | 2SE | Maximum age (Ma) | Mean age (Ma) | Minimum age (Ma) |
|---|---|---|---|---|---|---|
| TIS 6 | Mollusca | 0.708762 | 0.000006 | 15.77 | 15.67 | 15.51 |
| TIS 9 | Ostracoda | 0.708775 | 0.000009 | 15.53 | 15.40 | 15.14 |
| ŠKR 4 | *Trilobatus trilobus* | 0.708753 | 0.000008 | 15.96 | 15.83 | 15.69 |
| ŠKR 5 | Otolith | 0.708754 | 0.000006 | 15.91 | 15.81 | 15.71 |
| ID 14 | *Globigerinoides trilobus* | 0.708733 | 0.000008 | 15.45 | 15.17 | 14.87 |

***Table 5*** The $^{87}Sr/^{86}Sr$ values including standard errors converted into numerical ages using the regression curve LOWESS look-up Table version 6 (McArthur et al. 2020)

Based on the decreased $\delta^{18}O$ values in foraminifera and the presence of euryhaline planktic species, together with a decreased diversity of benthic foraminifera we suspect a freshwater influence. However, the observation of El Meknassi et al. (2018) controversially showed that riverine waters have generally higher $^{87}Sr/^{86}Sr$ values what is exactly the opposite case then in our data. Nevertheless, Benito et al. (2020) described decreasing of the $^{87}Sr/^{86}Sr$ values in coastal marine areas thanks to riverine input linked to weathering and erosion of the older carbonate rocks. It can be supported by the groundwater $^{87}Sr/^{86}Sr$ values from karst regions which strongly varied displaying even anomalously low values (Calligaris et al. 2018). Moreover, Schildgen et al. (2014) highlighted paleoclimatic

influences on the $^{87}Sr/^{86}Sr$-ratio as well, particularly in areas that are extensively underlain by carbonate rocks. The negative $^{87}Sr/^{86}Sr$ excursions occurred during the relative sea level drops, which generally coincide with arid conditions. Considerably lowered $^{87}Sr/^{86}Sr$ values are well known from the Mediteranean Messinian which has been interpreted as a relation to the gradual decrease of oceanic input thanks to the closure of the sea-ways and/or to the notable increase of freshwater input from river bodies(Rovieri et al. 2014 and reference therein). To summarize these observations, our data reflect a local $^{87}Sr/^{86}Sr$ signal influenced partly by the riverine input that drained the area composed of the older carbonate rocks. The comparison of our $^{87}Sr/^{86}Sr$ values with the already published data from the central Mediterranean region (Kocsis et al. 2008, Cornacchia et al. 2018) is ambiguous because we should use only data based on fossil biogenic carbonate. Sedimentary data from bulk sediment samples reflect different signal (Figure 10B). With respect to this premise our data can be compared with the values from the Monferrato area, Italy (Figure 10C).

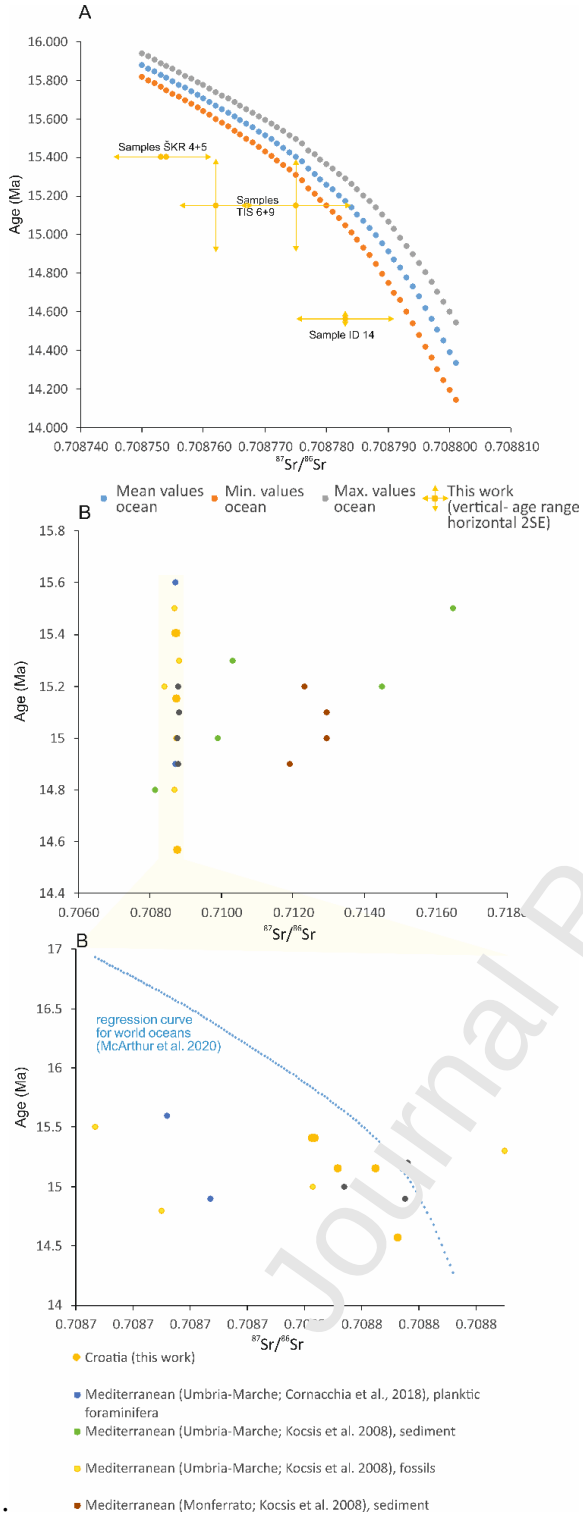


***Figure 10.*** *The comparison of the global $^{87}Sr/^{86}Sr$ oceanic-water signal (LOWESS look-up Table version 6; McArthur et al. 2020) with the data from the studied sections. (A) compared with the other $^{87}Sr/^{86}Sr$-values from the Mediterranean (Kocsis et al. 2008, Cornacchia et al. 2018). B – all data, C – detail of the plot B.*

5.2 Paleoenvironmental model

The distribution of the foraminiferal and calcareous nannoplankton assemblages, oxygen, and carbon isotope data, supported by palynology enable us to distinguish three distinct intervals with specific paleoenvironmental patterns corresponding to the individual studied sections (Figure 11) characterized by specific marine habitats, salinity, nutrient input and oxygen fluctuation.

5.2.1 Evolution of marine environment

The Langhian transgression apparently started after 15.4 Ma which is dating according to 40Ar/39Ar data of tuff horizonts of lacustrine deposits in underlaying of Badenian marine deposits of Mt. Medvedica (Corić et al. 2009, Markoviç 2017, Pavelić & Kovačić 2018). The area was inundated by a shallow strongly influenced by intensive rainfalls and river discharge, which agrees with regional larger climate instability during the early stage of the MCO (Crvgar et al., 2017) affected by Mi2 event (John et al. 2003; Auer et al. 2015). A rather high mean annual precipitation, exceeding today's values, dropped sharply up later around ~ 15.5 Ma years ago (Böhme et al. 2003, 2011). The isotopic composition of seawater together with the migrating organism are significantly influenced by rainfalls, which overlapped the signal that could determinated the origin of water masses.

The TIS section represented a shallow sea influenced by freshwater influx that flooded the area >15.5 Ma ago. The nannoplankton assemblages with the dominance of *Coccolithus. pelagicus* and helicosphaeras are considered to be an indicator of a near-shore environment (Ziveri et al. 2004, Galović, 2017) as well as dinocysts of *Cleistosphaeridium placacanthu*m which is often recorded in inner neritic, relatively marginal, and shallow settings (Zonneveld et al., 2013; Iakovleva, 2015). Together with other dinoflagellate cysts such as, *Polysphaeridium zoharyi*, *Spiniferites* spp., *Operculodinium* spp., *Hystrichokolpoma rigaudiae*, and *Lingulodinium machaerophorum* indicates an inner shelf environment with an upwards increasing connection to the open waters (Jaramillo and Oboh-Ikuenobe, 1999; Gedl, 1999).

Deepening of the Early Langhian sea connected with an environmental instability was recorded in the ŠKR section representing the time interval of ~ 15.4–15.34 Ma. Near-shore indicator *Coccolithus pelagicus* dominates also in nannoplanton assemblages of the ŠKR section. The exception is the

sample ŠKR 1, where it is replaced by a stress-tolerant *Reticulofenstra minuta* (cf. Wells and Okada, 1997; Flores et al., 1997; Kameo, 2002; Wade and Brown, 2006). Upwards, there is the increase of abundance in another stress marker in the form of mall *Helicoshaera walbersdorfensis*,indicates regional deepening (cf. Galović, 2020). This is accompanied by an increase in the diversity of planktic and benthic foraminiferal assemblages along with a decrease in their dominance as well as with increased abundance of reworked nannofossils in the samples ŠKR 7–9 (Figure 3D) which might be related to transgressive phase.

However, the values of these indices fluctuate, which might indicate a trend of stabilization establishing a normal marine environment intermittent by an episodic deterioration.

Overall, a progressive stabilization of a fully developed marine environment could reflect a continuation of marine transgression as well as decreased rainfall periods ~ 14.4 Ma as reported in Böhme et al. (2011). However, a still shallow water environment and mixed water column did not allow immigration and survival of planktic foraminifera from the *Praeorbulina* lineage in the study region. Benthic assemblages are predominantly stenohaline and reflect changes indicating an episodic input of nutrients. Generally, a rather eutrophic environment was persistent from the previous time interval. The paleoenvironmental conditions of the southwestern margin of the Central Paratethys clearly differ from the Mediterranean ones.

The provided biostratigraphic constraints confirm the conclusions provided by Brlek et al. (2020) based on high-precision geochronology that marine flooding of some parts of the North Croatian Basin (e.g., TIS and ŠKR sections on Mt. Požeška Gora) occurred already during the NN4 zone and ~0.4 Ma before the generally accepted timing of the initial the North Croatian Basin flooding interpreted approximately at 15 Ma (Ćorić et al., 2009; Mandic et al., 2012, 2019a, b; Sant. et a., 2017, 2019; Pavelić and Kovačić, 2018; Marković et al. 2021). This indicates either that the initial transgression might have been diachronous across the other Central Paratethyan basins (Bartol, 2009; Hohenegger et al., 2009; Avanić, 2012; Kováč et al., 2017, 2018; Sant et al., 2017, 2019, 2020;; Holcová et al., 2018; Ivančič et al., 2018; Mandic et al., 2019a, b, c; Avanić et al., 2021; Premec- Fuček et al., submitted). This calls for further derivation of high precision and quality geochronological, chemo- and bio-

stratigraphic data, which should enable more reliable interpretations of crucial events in the evolution of the Central Paratethys Sea and the sedimentary basins it affected, such as the timing and causes (eustatic vs. tectonic) of Badenian Sea(s) and onsets of particular flooding(s).

The ID section represents a well-developed marine environment with a summer stratification in the interval ~ 14.56 – 14.34 Ma (FO *O.suturalis* and LO *H. waltrans*) where marine deposits represent the widespread (on the North Croathian Basin and Central Paratethys scale) "late-Langhian" Central Paratethys flooding and the installation of the "Middle Badenian Sea" before and after 14.6 Ma (NN5 Zone; Ćorić et al., 2009; Mandic et al., 2012, 2019a, b; Sant et al., 2017, 2019, 2020; Kovač et al., 2017, 2018; Ivančič et al., 2018; Pavelić and Kovačić, 2018; Rybar et al., 2019; Marković et al. 2021) i.e. after the FO *O. suturalis* (Hoheengger et al. 2014; Siedl et al. 2020; Harzhauser et al. 2020). The Central Paratethys marine environments reached the ID lacustrine/brackish basement (lower intervals barren of marine micro- and nannofossils) later than at the TIS and ŠKR sections probably due to the local tectonic and paleomorphological paleorelief North Croatian Basin-scale settings (see Brlek et al., 2018). The composition of the planktic assemblages shows different surficial waters in comparison with the older Langhian interval. Warm water *Reticulofenstra minuta* dominates in the calcareous nannoplankton assemblages indicating a deterioration of surface waters (e.g. salinity and/or nutrient load oscillations; Wells and Okada 1997; Flores et al., 1997; Kameo, 2002; Wade and Brown, 2006). The dominance of *R. minuta* is a regional phenomenon since it is typical for calcareous nannoplankton assemblages of the Middle Badenian in the whole Central Paratethys marine realm (e.g., Ćorić and Hohenegger, 2008; Pezelj et al., 2013; Doláková et al., 2014; Holcová et al., 2015; Nehyba et al., 2016; Mandic et al. 2019b, c) and confirms the Middle Miocene Climatic Optimum.

Overall, the second Langhian transgression enabled the presence of *Praeorbulina* and *Orbulina* due to the formation of warm summer surficial waters. The connection between these realms might be of two types: an unknown direct connection (Rögl, 1998) or exclusively via the Eastern Mediterranean to the southwestern margin of the Central Paratethys (Holcová et al., 2018). Moreover, the dominance of *Reticulofenestra minuta* suggests a unification of the Central Paratethys surficial warm waters. A well-developed seasonality can be interpreted from the co-occurrence of seasonal aspects in the planktic

foraminiferal assemblages and it probably reflects the initiation of the Middle Miocene Climatic transition. The decrease of nutrients accompanied with the decrease of numbers of suspension feeders together with the oxygen isotope signal might be linked with the decline of rainfall period compared to the older studied sections.

5.2.2 Salinity fluctuation

In all studied sections, some indices were recorded that demonstrate fluctuations in salinity in the paleoenvironment. In TIS section, the predominant *H. carteri* in the calcareous nannoplankton assemblages (TIS 4–5) can tolerate oscillations of salinity (cf. Flores et al., 1997; Hidalgo et al., 2004; Triantaphyllou et al., 2009; Cros, 2001) similar to increasing abundance of *Valvulineria* (cf. Bergamin et al., 1999; Frezza et al. 2005; Frezza et al. 2009; Hayward et al. 2010) in benthic assemblages of ŠKR section (ŠKR 4) and *Reticulofenestra minuta* (cf. Wells and Okada 1997; Flores et al., 1997; Kameo, 2002; Wade and Brown, 2006) in ID section.

These agree well with the isotopic data from the sections. Anomalously low values of $\delta^{18}O$ of small globigerinids ranging from –6.7 ‰ in TIS section and in the scale of 4.9 ‰ to –3.1 ‰ in ŠKR section probably points to surface waters with lower salinity because of freshwater input. . It agrees with the climatic situation during the Miocene Climatic Optimum, including climate warming, heavy rainfalls and a high riverine influx into marginal marine basins (Utescher et al. 2007; Brush et al. 2011).

5.2.3 Carbon flux, nutrients and oxygen content

The paleoenvironments were characterized by a significant flow of nutrients. Calcareous plankton recorded in TIS section, which is dominated by planktonic foraminifera *G. tarchanensis–T. quinqueloba*, points to eutrophic surficial waters with a high nutrient content (cf. Okada and McIntyre, 1979; Sautter, Sancetta, 1991; Ottens and Nederbragt, 1992; Sauter and Sencetta, 1992; Winter et al., 1994; Cachao and Moita, 2000; Spezzaferri and Rögl, 2003; Beldean et al., 2012; Wilson, 2005) as well as a common occurrence of the peridinoid dinoflagellate cysts (*Lejeunecysta* spp., *Sumatradinium* spp., *Selenopemphix* spp.; cf. Matsuoka, 1987) in the lower part of the TIS section Increased

planktonic markers of environmental stress were recorded in the upper part of this section. Oportunistic *G. uvula* (Kennett and Srinivasan, 1983; Schiebel and Hemleben, 2017) displaced *G. tarchanensis–T. quinqueloba* and the *C. pelagicus* assemblages were substituted by the *Helicosphaera* one in TIS 4–5. The predominant *H. carteri* in the calcareous nannoplankton assemblages is an opportunistic species that can tolerate oscillations of salinity and an increased, frequent terrigenous input near the riverine discharge (Flores et al., 1997; Colmenero-Hidalgo et al., 2004; Triantaphyllou et al., 2009; Cros, 2001). Changes in planktic assemblages correspond with an increased abundance of *Valvulineria* at the seafloor (ŠKR 4) that could support the presumed increased terrigenous influx, decreased oxygen concentration and salinity (cf. Bergamin et al., 1999; Frezza et al. 2005; Frezza et al. 2009; Hayward et al. 2010) as well as common foraminiferal species *Bolivina hebes* which is also often considered stress-tolerant (Spezzaferri and Rögl, 2005, Pezejl et al., 2013). Nutrient-rich environment is also indicate by $\delta^{13}C$ values of small globigerinids ranking from ~ -1.7 ‰ to -1.1‰. It is in accordance with the river runoff causing eutrophication to which these small globigerinids abruptly respond because of their high-nutrient preference and association with regions with a surface-water instability (e.g. Al-Sabouni et al., 2007; Schmidt et al., 2004a).

This is in contrast with the benthic assemblages with no clearly eutrophic taxa. In the lower part of the section, the sea-floor environment was settled by *Cibicidoides* a marker of oxic conditions and suspension feeder (Murray 2014). Subsequently, there is an increase in the abundance of infaunal bolivinas applying to occasional hypoxic conditions at the bottom (Fig. 7A-B) as well. The $\delta^{13}C$ values of *Cibicidoides* are positive ranging from ~ +0.4 ‰ to +1.6 ‰ with the main cluster between +0.5 ‰ to +1 ‰. It probably reflects a rather nutrient-scarce environment. *Cibicidoides* sp. is commonly considered as an epifaunal species living attached to various substrates (hard substrates as well as biotic substrates) or living in the topmost sediment layer (e.g. Murray, 2006; Schmiedl et al., 2000). The higher $\delta^{13}C$ suggest that in this case the species probably did not occupy the sediment layer because they would have to respond to the higher amount of organics and detritus at the sea-floor associated with the eutrophication of surficial waters. This species probably occupied bottom waters attached to a substrate and experienced an environment that was already relatively depleted in $^{12}C$ and thus acquired the higher $\delta^{13}C$ values, which is a common situation in waters with high primary

productivity. This could be also a response to a decreased oxygen content within the topmost sediment layer. Since we observe this phenomenon with relation to the epifaunal species it also suggests that this species lived in a relatively shallower well-mixed environment.

In ŠKR section, the planktonic foraminiferal assemblages characterize surficial waters dominated by tenuitellids and *G. uvula.* Tenuitellids are known to occupy mixed shallow waters above the thermocline (Schiebel and Hemleben, 2017) with surface-water instability (Al-Sabouni et al. 2007). Isotope paleobiology data suggest that this group lives in the topmost surficial layer (Majewski, 2003), or perhaps slightly deeper in comparison with the other small foraminiferal species (Pearson and Wade, 2009). The abundance of stress-tolerant tenuitellids and *G. uvula* upwards the section decreases and they are being replaced by *Globigerina* div. sp., together with an increasing diversity it probably indicates diminishing of stress factors in surficial waters. Isotopic data of *Globigerina bulloides/praebulloides*, which has a majority of the $\delta^{18}O$ values in an interval between ~ —1.8 ‰ to —0.8 ‰, whereas the $\delta^{13}C$ values are between —0.1 ‰ to +0.8 ‰, reflect a mixed water column with adequate nutrient availability. It is well-known that *Globigerina bulloides* tolerates a wide range of temperatures, but prefers high-nutrient levels (e.g. Hemleben et al., 1989; Schiebel et al., 1997).

Variability in the composition of the benthic foraminiferal assemblages suggests episodic environmental variances at the seafloor. A oxiphylic *Cibicidoides* together with *Fontbotia* and *Heterolepa* dominate mainly in the lower part of the sections and represent passive suspension feeders (Murray, 2014). Moreover, *Heterolepa* preferably lives on organic-rich substrates (Debenay and Redois, 1997). These suspension-feeding genera were episodically replaced by monoserial foraminifera and infaunal detrivore species such as *Melonis, Pullenia*, and *Bolivina.* It clearly suggests episodic oscillations of the availability of nutrients in suspension. Generally, all the studied taxa indicate eutrophic conditions at the bottom waters and seafloor.

Focusing on the benthic species we have representatives of epifaunal as well as infaunal species. *Cibicidoides ungerianus* represents an epifaunal species and it exhibits an extensive range of the $\delta^{18}O$ as well as $\delta^{13}C$ values, which is probably related to various life strategies this species could thrive in as already discussed for the previous section. Regarding the infaunal species, there are *Melonis*

*pompilioides* with the $\delta^{18}O$ values ranging from ~ –2.4 ‰ to –0.9 ‰ and *Pullenia bulloides* with the $\delta^{18}O$ values between ~ –2.6 ‰ to –0.4 ‰. The $\delta^{13}C$ values range from ~ –1 ‰ to –0.5 ‰ and ~ –1.1 ‰ to –0.1 ‰, respectively. Both species have very similar isotopic patterns, which suggest a certain similarity in their infaunal habitat. *Melonis* sp. is often considered as a rather static intermediate infaunal species with a preference for higher nutrient levels (e.g. Mackensen et al., 2000; Schmiedl et al., 2000), while *Pullenia* is often considered as a shallow infauna tolerant to the intermediate flux of nutrients and a pulsed-food supply (e.g. Gupta and Thomas, 1999; Soma De and Gupta, 2010he $\delta^{13}C$ values are very comparable for both species, indicating they occupied related ecological niches and pointing to a relatively high nutrient supply. It could be possibly linked with the situation in the upper part of the water column, where there are marks of high nutrient levels such as small globigerinids and the presence of *Globigerina bulloides/praebulloides*. The eutrophication events could be associated with a pulse of a food supply to the sea floor, which is then reflected in the $\delta^{13}C$ data of the infaunal species. Furthermore, several studies reported that within the topmost sediment layer a high content of organics could cause variations in factors such as pH affecting the microenvironment and population dynamics of benthic communities, which all together could result in shifts in their geochemical signals (e.g. Schenner et al., 2019; Mackensen et al., 2000; Schmiedl et al., 2000).

The re-deterioration of surface water ((e.g. salinity and/or nutrient load oscillations) indicates the increasing dominance of warm water calcareous nannoplankton species *Reticulofenstra minuta* (cf. Wells and Okada 1997; Flores et al., 1997; Kameo, 2002; Wade and Brown, 2006) in ID section. The dominance of *R. minuta* is a regional phenomenon since it is typical for calcareous nannoplankton assemblages of the Middle Badenian in the whole Central Paratethys marine realm (e.g., Ćorić and Hohenegger, 2008; Pezelj et al., 2013; Doláková et al., 2014; Holcová et al., 2015; Nehyba et al., 2016; Mandic et al. 2019b, c) and confirms the Middle Miocene Climatic transition.

The assemblages of planktic foraminifera differ by the larger size and by the highest diversity in comparison with the previous intervals. The *Globigerinoides trilobatus-Globigerina paebulloides* assemblage is characteristic for this interval. *G. bulloides* and smaller G. *praebulloides* are considered

as high-productivity markers related to a warming period inducing the phytoplankton bloom while *Globigerinoides, Orbulina,* and *Praeorbulina* indicate a presence of warm, summer, oligotrophic surficial waters (Reynolds and Thunell, 1985; Hemleben et al., 1989; Spezzaferri, 1995; Ohta et al., 2003; Schiebel and Hemleben, 2017; Jonkers et al., 2019; Incarbona et al., 2019). Co-existence of these taxa can be linked with increased and well-developed connectivity and the climate peak as well recorded in the Paratethys between 14.5 – 13.8 Ma (Methner et al. 2020) .

Monoserial foraminifera, dominating in the benthic assemblages, indicate a nutrient-rich environment. Together with the other common taxa such as *Lenticulina* and *Bolivina* represent a shallow to intermediate infauna in muddy substrates (Spezafferri and Rogl, 2003; Bhaumik et al., 2011; Murray 2014). Moreover, the decrease of the presence of suspension feeders (cibicidoids) probably suggests a scarcity of nutrients in suspension or an increased competition at the seafloor.

From stable carbon and oxygen isotopes, the ID section represents a well-developed marine environment different from the TIS and ŠKD sections. There is a presence of *Globigerinoides trilobatus* with the $\delta^{18}O$ values ranging from ~ –2.4 ‰ to –1.4 ‰ and with the $\delta^{13}C$ ranging from ~ +2.1 ‰ to +3.1 ‰, which clearly documents warm oligotrophic surficial waters for which is this species characteristic (e.g. Reynolds and Thunell, 1985; Hemleben et al., 1989; Chapman, 2010; Schiebel and Hemleben, 2005), likely representing summer seasons. *Globigerina bulloides/praebulloides* exhibits a broad range of the $\delta^{18}O$ values between ~ –2.7 ‰ to –0.5 ‰ together with the $\delta^{13}C$ range from ~ –0.8 ‰ to +0.8 ‰ apparently representing different seasons, where there are sufficient nutrient inputs but the water temperature is highly variable because this species is typical for its high-nutrient preference and tolerance to a wide range of temperatures. It is very probable that the samples are a mix of different populations from various seasons (e.g. Deusser et al., 1981; Schiebel et al., 1997). The epifaunal benthic *Cibicidoides ungerianus* $\delta^{18}O$ values range between ~ –2.6 ‰ to –0.3 ‰ with the $\delta^{13}C$ range from ~ –0.6 ‰ to +1.3 ‰, which is again a very extensive range of values that could be explained by the high variability of life-strategies this species could experience. The infaunal species in the ID section are represented by *Melonis pompilioides* and *Gyroidinoides* sp., where *Melonis* represents an intermediate static infauna with high nutrient

preferences, whereas *Gyroidinoides* sp. is a shallow infaunal species with low food demands (e.g. Sjoerdsma and Van der Zwaan, 1992; Sen Gupta and Machain-Castillo, 1993; Mackensen et al., 2000; Schmiedl et al., 2000). *Melonis pompilioides* exhibits somewhat low $\delta^{18}O$ values from ~ –2.6 ‰ to +0.3 ‰ with the majority of values within a cluster ranging from ~ –1.3 ‰ to +0.3 ‰, which suggest relatively warm bottom waters. The $\delta^{13}C$ values represent a narrow interval from –0.5 ‰ to +0.2 ‰ pointing to an intermediate nutrient availability that is lower compared to the ŠKR section. *Gyroidinoides* sp. displays a high similarity with the $\delta^{18}O$ ranging between ~ –1.5 ‰ to +0.6 ‰ and with the $\delta^{13}C$ ranging from ~ –0.7 ‰ to +0.6 ‰, which again possibly indicates relatively warm bottom waters with an intermediate nutrient availability probably originating in a summer or fall seasons considering the productivity patterns for mid-latitudes.

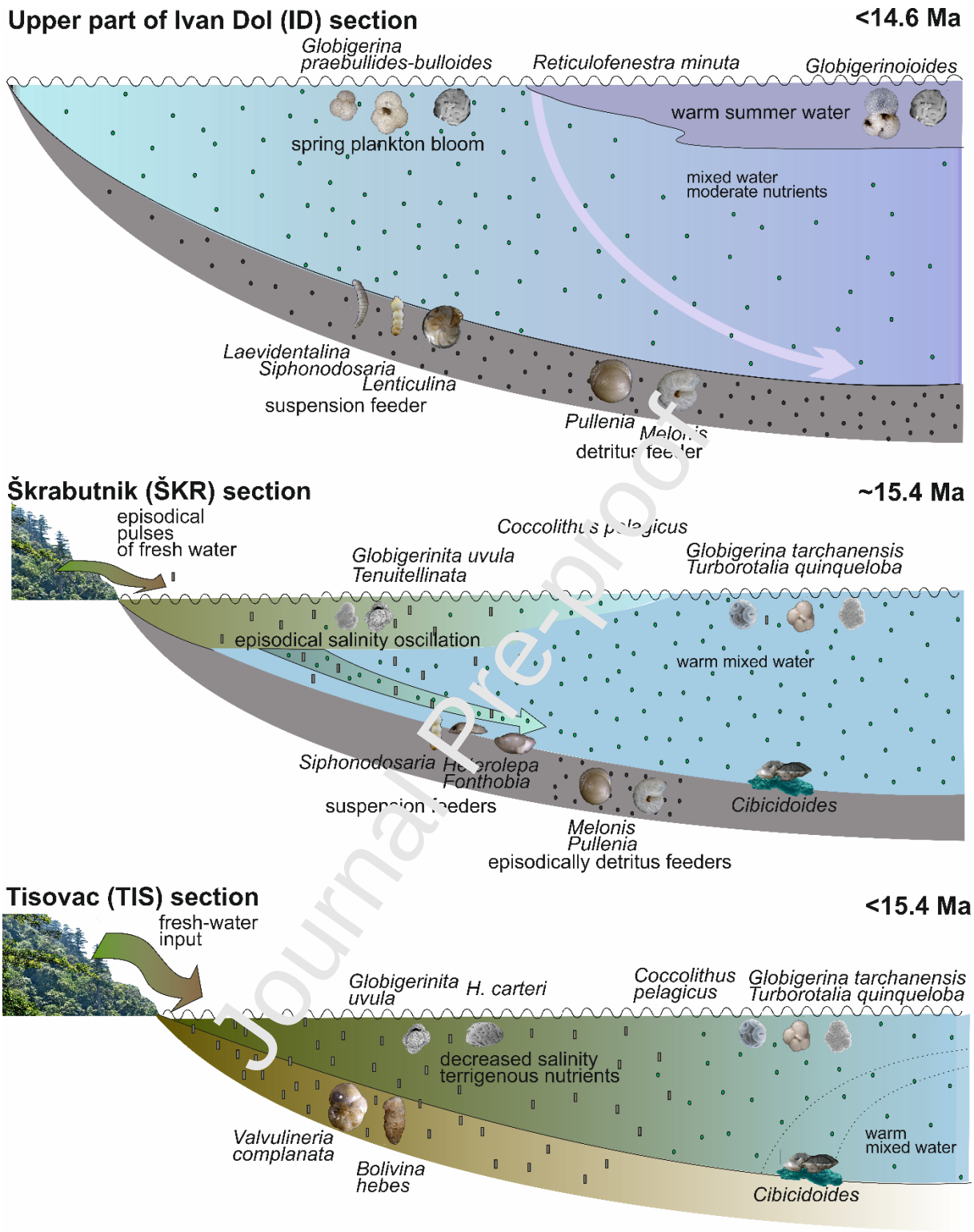


***Figure 11*** *Model of the paleoenvironmental patterns in the southwestern part of the Central Paratethys Sea during the peak of the Miocene Climatic Optimum*

## Conclusions

We synthesized a paleoenvironmental model for the southwestern margin of the Paratehys and evaluated an influence of global climatic signal on the local evolution in this model during the time interval corresponding with the Miocene Climate Optimum (~ 15.9–14.9 Ma).

The age model is based on the Strontium Isotope Stratigraphy compared with the already published radiometric datums. It shows the heterochrony of planktic foraminifera bioevents in the interval between 15–15.9 Ma in the Paratethys and the Mediterranean, which was probably caused by the decreased quality of the Paratethyan surficial waters (decreased salinity).

The first marine flooding can be correlated with the Burdigalian/Langhian boundary (15.974 Ma) and was represented by a rather shallow, high-nutrient sea which was greatly affected by the freshwater input and represents an environment with a relatively well-mixed water column, high-nutrient availability, and somewhat warm bottom waters. It clearly indicates the decisive influence of wet climate on water masses in a shallow sea, which agrees well with a climate instability and continental climatic model (thermal peaks) during the MCO in Central Europe.

During the continued flooding (~15.5 Ma), there was a stabilization of the stenohaline environment, but the presence of a mixed water column of still shallower environment did not allow migration and survival of the representatives of the *Praeorbulina* lineage.

The last phase of the marine flooding (< 15.3 Ma) is represented by typical seasonal stratification during summer seasons with mesotrophy generated primarily in summer seasons with respect to the position of the locality in the mid-latitudes The timing of the immigration of the representatives of the *Praeorbulina-Orbulina* lineage suggests that surficial waters were probably influenced by the Indian Ocean surface waters. The bottom waters became warmer, which evokes their origin from the lower latitudes.

## Acknowledgments

This work has been supported by the following projects: Czech Science Foundation GA20-05872S to KH; the institutional support was provided by the research program RVO 67985831; PROGRES Q45 and by the Center for Geosphere Dynamics UNCE/SCI/006 (Charles University). It was also supported in part by Croatian Science Foundation under the project "Miocene syn-rift evolution of the (Carpathian-Pannonian Region): a multi-proxy approach, correlation and integration of sedimentary and volcanic record" (PYROSKA, HRZZ UIP-2019-04-7761), and Internal Fund of Faculty of Education VaV_PdF_2021_04. Additionally, thanks to Mirjana Miknić for field support.

The authors would also like to thank Oleg Mandic and an anonymous reviewer for their constructive suggestions and insightful comments.

## Declaration of interests

☒ **The authors declare that they have no known competing financial interests or personal relationships that could have appeared to influence the work reported in this paper.**

☐The authors declare the following financial interests/personal relationships which may be considered as potential competing interests:

**References**

Allen, M. B., Armstrong, H. A., 2008. Arabia–Eurasia collision and the forcing of mid-Cenozoic global cooling. PaleoPaleogeography, PaleoPaleoclimatology, PaleoPaleoecology, 265(1-2), 52-58. http://dx.doi.org/10.1016/j.palaeopaleo.2008.04.021

Al-Sabouni, N., Kucera, M., Schmidt, D. N., 2007. Vertical niche separation control of diversity and size disparity in planktic foraminifera. Marine Micropaleontology, 63, 1-2, 75-90. https://doi.org/10.1016/j.marmicro.2006.11.002

Argentino, C., Reghizzi, M., Conti, S., Fioroni, C., Fontana, D., Salocchi, A.C., 2017. Strontium isotope stratigraphy as a contribution for dating Miocene shelf carbonates (S. Marino Fm., Northern

Apennines): Research in Paleontology and Stratigraphy, 123, p. 39-50. http://dx.doi.org/10.13130%2F2039-4942%2F8017

Armentrout, J. M., Echols, R. J., Lee, T. D., 1991. Patterns of foraminiferal abundance and diversity: implications for sequence stratigraphic analysis. In: AAPG Bulletin (American Association of Petroleum Geologists, USA), 75(CONF-910403-).

Auer, G., Piller, W. E., & Harzhauser, M. (2015). Two distinct decadal and centennial cyclicities forced marine upwelling intensity and precipitation during the late Early Miocene in central Europe. Climate of the Past, 11(2), 283-303.

Avanić, R ., 2012. Litostratigrafske jedninice donjeg miocena sjeverozapadne Hrvatske. Dissertation, University of Zagreb, Zagreb, 162 pp.

Avanić, R., Pavelić, D., Pécskay, Z., Miknić, M., Trijar, D., Wacha, L., 2021. Tidal deposits in the Early Miocene Central Paratethys: the Vučji Jarak and Čemernica members of the Macelj formation (NW Croatia). Geologica Croatica, 74, 41–56. https://doi.org/10.4154/gc.2021.06

Aziz, H. A., Di Stefano, A., Foresi, L. M., Hilgen, F. J., Iaccarino, S. M., Kuiper, K. F., Liler, F., Salvatorini, G., Turco, E., 2008. Integrated stratigraphy and 40Ar/39Ar chronology of early Middle Miocene sediments from DSDP Leg 42A, Site 372 (Western Mediterranean). PaleoPaleogeography, PaleoPaleoclimatology, PaleoPaleoecology, 257(1-2), 123-138. https://doi.org/10.1016/j.paleopaleo.2007.09.013

Bakrač, K., Koch, G., Sremac, J.,2012. Middle and Late Miocene palynological biozonation of the south-western part of Central Paratethys (Croatia). Geologia Croatica, 65(2), 207-222. http://dx.doi.org/10.4154/gc.2012.12

Balázs, A., Matenco, L., Magyar, I., Horváth, F., Cloething, S., 2016. The link between tectonics and sedimentation in back-arc basins: New genetic constraints from the analysis of the Pannonian Basin. Tectonics, 35, 1526–1559. https://doi.org/10.1002/2015TC004109

Barker, S., Greaves, M., Elderfield, H., 2003. A study of cleaning procedures used for foraminiferal Mg/Ca paleothermometry. Geochem. Geophys. Geosyst. 4 (9), 8407. http://dx.doi.org/10.1029/2003GC000559.

Bartol, M., 2009. Middle Miocene calcareous nannoplankton of NE Slovenia (western Central Paratethys). Založba ZRC/ZRC Publishing, Ljubljana, 136 pp.

Beldean, C., Filipescu, S., Balc, R., 2012. Paleoenvironmental and biostratigraphic data for the Early Miocene of the north-western Transylvanian Basin based on planktic foraminifera. Carpathian Journal of Earth and Environmental Sciences, 7(1), 171-184.

Benito, M.I., Suarez-Gonzalez, P., Quijada, I.E. , Sonia Campos-Soto, S., Rodríguez-Martínez , *M.* 2020: Constraints of applying strontium isotope stratigraphy in coastal and shallow marine environments: insights from Lower Cretaceous carbonates deposited in an active tectonic setting (N Iberian Basin, Spain). *J Iber Geol* **47,** 151–169 (2021). ttps://doi.org/10.1007/s41513-020-00142-z

Böhme, M., 2003. Miocene Climatic Optimum: evidence from Lower vertebrates of Central Europe. PaleoPaleogeography, PaleoPaleoclimatology, PaleoPaleoecology 195, 389–401. https://doi.org/10.1016/S0031-0182(03)00367-5

Böhme, M., Winklhofer, M., Ilg, A., 2011. Miocene precipitation in Europe: Temporal trends and spatial gradients. PaleoPaleogeography, PaleoPaleoclimatology, PaleoPaleoecology 304(3-4), 212-218. https://doi.org/10.1016/j.paleopaleo.2010.09.028

Bartol, M. 2009. Middle Miocene calcareous nannoplankton of NE Slovenia (western Central Paratethys). Založba ZRC/ZRC Publishing, Ljubljana, 136 pp.

Bosio, G., Malinverno, E., Collareta, A., Di Celma, C., Gioncada, A., Parente, M., Berra, F., Marx, F.G., Vertino, A., Urbina, M., Bianucci, G.2020. Strontium isotope stratigraphy and the thermophilic fossil fauna from the middle Miocene of the East Pisco Basin (Peru). Journal of South American Earth Studies, 97. https://doi.org/10.1016/j.jsames.2019.102399

Brlek, M., Kutterolf, S., Gaynor, S., Kuiper, K., Belak, M., Brčić, V.,, Holcová K., Wang ,K.L,, Bakrač, K., Hajek-Tadesse, V., Mišur, I., Horvat, M., Šuica, S., Schaltegger, U. 2020. Miocene syn-rift evolution of the (Carpathian-Pannonian Region): new constraints from Mts. Kalnik and Požeška gora volcaniclastic record with regional implications. International Journal of Earth Sciences, 109, 2775–2800. http://dx.doi.org/10.1007/s00531-020-01927-4

Brlek, M., Gaynor, S.P., Mongelli, G., Bauluz, B., Sinisi, R., Brčić, V., Peytcheva, I., Mišur, I., Tapster, S., Trinajstić, N., Laita, E., Yuste, A., Šuica, S., Grizelj, A., Kukoč, D., Schaltegger, U., 2021. Karst bauxite formation during Miocene Climatic Optimum (central Dalmatia, Croatia): mineralogical, compositional and geochronological perspectives. International Journal of Earth Sciences, 1-24. https://doi.org/10.1007/s00531-021-02091-z

Bryant, J. D., Jones, D. S., & Mueller, P. A. (1995). Influence of freshwater flux on 87Sr/86Sr chronostratigraphy in marginal marine environments and dating of vertebrate and invertebrate faunas. *Journal of Paleontology*, *69*(1), 1-6.

Bruch, A. A., Utescher, T., & Mosbrugger, V. (2011). Precipitation patterns in the Miocene of Central Europe and the development of continentality. Palaeogeography, Palaeoclimatology, Palaeoecology, 304(3-4), 202-211.

Cachao, M., Moita, M. T., 2000. *Coccolithus pelagicus*, a productivity proxy related to moderate fronts off Western Iberia. Marine Micropaleontology, 39(1-4), 131-155. http://dx.doi.org/10.1016/S0377-8398(00)00018-9

Calligaris, C., Mezga, K., Slejko, F. F., Urbanc, J., & Zini, L. (2018). Groundwater characterization by means of conservative (d18O and d2H) and non-conservative (87Sr/86Sr) isotopic values: The Classical Karst Region aquifer case (Italy-Slovenia). *Geosciences, 8*, 321–346.

Colmenero-Hidalgo, E., Flores, J. A., Sierro, F. J., Bárcena, M. A., Löwemark, L., Schönfeld, J., Grimalt, J. O., 2004. Ocean surface water response to short-term climate changes revealed by coccolithophores from the Gulf of Cadiz (NE Atlantic) and Alboran Sea (W Mediterranean).

PaleoPaleogeography, PaleoPaleoclimatology, PaleoPaleoecology, 205(3-4), 317-336. http://dx.doi.org/10.1016/j.paleopaleo.2003.12.014

Ćorić, S., Pavelić, D., Rögl, F., Mandic, O.,, Vrabac S.,, Avanić R., Jerković, L., Vranjković, A., 2009. Revised Middle Miocene datum for initial marine flooding of North Croatina Basins (Pannonian Basin Systems, Central Paratethys). Geologica Croatica, 62, 31–43. http://dx.doi.org/10.4154/GC.2009.03

Ćorić, S., Hohenegger, J. 2008. Quantitative analyses of calcareous nannoplankton from Baden-Sooss section (Austria). Geologica Carpathica, 59, 447—460.

Cornacchia, I., Agostini, S., Brandano, M., 2018. Miocene Oceanographic Evolution Based on the Sr and Nd Isotope Record of the Central Mediterranean. Paleoceanography and Paleoclimatology 33, 31–47. https://doi.org/10.1002/2017PA003198

Cros, L., 2001. Planktic coccolithophores of the NW Mediterranean. Doctoral dissertation, Universitat de Barcelona. Barcelona.

de Leeuw, A., Tulbure, M., Kuiper, K.F.. Melinte-Dobrinescu, M.C., Stoica, M., Krijgsman, W., 2018. New $^{40}Ar/^{39}Ar$, magnetostratigraphic and biostratigraphic constraints on the termination of the Badenian Salinity Crisis: Indications for tectonic improvement of basin interconnectivity in Southern Europe. Global and Planetary Change, 169, 1–15. http://dx.doi.org/10.1016/j.gloplacha.2018.07.001

De, S., Gupta, A. K., 2010. Deep-sea faunal provinces and their inferred environments in the Indian Ocean based on distribution of recent benthic foraminifera. PaleoPaleogeography, PaleoPaleoclimatology, PaleoPaleoecology 291(3–4), 429-442. https://doi.org/10.1016/j.paleopaleo.2010.03.012.

Debenay, J. P., Redois, F., 1997. Distribution of the twenty-seven dominant species of shelf benthic foraminifers on the continental shelf, north of Dakar (Senegal). Marine Micropaleontology, 29(3), 237–255. https://doi.org/10.1016/S0377-8398(96)00034-5

del Río, C.J., Martínez, S.A., McArthur, J.M., Thirlwall, M.F., Pérez, L.M., 2018. Dating late Miocene marine incursions across Argentina and Uruguay with Sr-isotope stratigraphy. Journal of South American Earth Sciences, 85, 312-324. http://dx.doi.org/10.1016/j.jsames.2018.05.016

Deusser, W.G., Ross, E.H., Hemleben, C., Spindler, M., 1981. Seasonal changes in species composition, number, mass, size, and isotopic composition of planktic foraminifera settling into the deep Sargasso Sea. PaleoPaleogeography, PaleoPaleoclimatology, PaleoPaleoecology, 33, 103–127. https://doi.org/10.1016/0031-0182(81)90034-1

Di Stefano, A., Foresi, L. M., Lirer, F., Laccarino, S. M., Turco, E., Amore, F. O., Mazzei, R. Morabito, S. Salvatorini, G. Aziz, H.A.,2008. Calcareous plankton high resolution biomagnetostratigraphy for the Langhian of the Mediterranean area. Rivista Italiana di Paleontologia e Stratigrafia, 114(1), 51. https://doi.org/10.13130/2039-4942/6269

El Meknassi, S., Dera, G., Cardone, T., De Rafélis, M., Brahmi, C., & Chavagnac, V. (2018). Sr isotope ratios of modern carbonate shells: Good and bad news for chemostratigraphy. Geology, 46(11), 1003-1006. https://doi.org/10.1130/G45380.1

Fan, T., Yu, K., Zhoa, J., Xu, Shendong, Zhang, Y., Wang, R., Wang, Y., Feng, Y., Bian, L., Qian, H., Lao, W., 2020. Strontium isotope stratigraphy and paleomagnetic age constraints on the evolution history of coral reef islands, northern South China Sea. GSA Bulletin, 132, p. 803-816. https://doi.org/10.1130/B35088.1

Flores, J. A., Sierro, F. J., 1997. Reevised technique for calculation of calcareous nannofossil accumulation rates. Micropaleontology, 43(3), 321-324. https://doi.org/10.2307/1485832

Flower, B. P., J. P. Kennett,1994. The middle Miocene climatic transition: East Antarctic ice sheet development, deep ocean circulation and global carbon cycling, PaleoPaleogeography, PaleoPaleoclimatology, PaleoPaleoecology, 108, 537–555. https://doi.org/10.1016/0031-0182(94)90251-8.

Frezza, V., Bergamin, L., & Di Bella, L. (2005). Opportunistic benthic foraminifera as indicators of eutrophicated environments. Actualistic study and comparison with the Santernian middle Tiber Valley (Central Italy). *Bollettino-societa paleontologica Italiana*, *44*(3), 193.

Frezza, V., & Carboni, M. G. (2009). Distribution of recent foraminiferal assemblages near the Ombrone River mouth (Northern Tyrrhenian Sea, Italy). *Revue de micropaléontologie*, *52*(1), 43-66.

Gradstein, F. M., Ogg, J. G., 2020. The chronostratigraphic scale. In: Gradstein F. M., Ogg J. G., Schmitz M.D., Gabi M. Ogg G. M. (eds.), Geologic Time Scale, Elsevier, 2020, pp. 21-32.

Grygar, T. M., Hošek, M., Mach, K., Schnabl, P., & Martinez, M. (2017). Climatic instability before the Miocene Climatic Optimum reflected in a Central European lacustrine record from the Most Basin in the Czech Republic. Palaeogeography, Palaeoclimatology, Palaeoecology, 485, 930-945.

Gupta, A.K., Thomas, E. 1999. Latest Miocene through Pleistocene paleoceanographic evolution of the northwestern Indian Ocean (DSDP Site 219 : global and regional factors. Paleoceanography 14, 62-73 pp. https://doi.org/10.1029/1998PA900006

Hajek-Tadesse, V., Belak, M., Sremac, J., Vrsaljko D., Wacha, L., 2009. Early Miocene ostracods from the Sadovi section (Mt Požeška Gora, Croatia). Geologica Carpathiaca, 60, 251–262.

Halamić, J., Belak,. M,, Pavelić D., Avanić, R.,, Filjak R.,, Šparica M.,, Brkić M., Kovačić, M., Vrsaljko, D., Banak, A., Crnko, J., 2019. Basic Geological Map 1:50.000. Sheet Požeška Gora. Croatian Geological Survey, Zagreb.

Hammer, Ø., Harper, D.A.T., Ryan, P.D., 2001. PAST: Paleontological statistics software. http://priede.bf.lu.lv/ftp/pub/TIS/datu_analiize/PAST/2.17c/download.html

Hemleben, C., Spindler, M., Anderson, O.R., 1989. Modern Planktic Foraminifera. Springer, New York, 363 pp.

Hernitz Kučenjak, M.,, Premec Fućek V., Krizmanić Tadej, J., Zlatar, S., Matošević, M., 2018. Karpatian and Badenian transgressions in Croatian part of the Pannonian Basin System (biostratigraphy and paleopaleoenvironments). Forams 2018, Temporary Abstract Collection, Edinburgh, pp 273–274.

Hernitz-Kučenjak, M., Premec-Fuček,.V., Galović, I., Hajek-Tadesse, V., Krizmanić, K., Matošević, M., Mikša, G., Zlatar, S., Pecimotika, G., 2019. Paleoecology and paleoenvironment of the Upper Karpatian-Lower Bedenian Sedimentary Succession from SE Medvednica Mt., Croatia. In: Horvat, M., Matoš, B.,, Wacha L. (Eds.), 6th Croatian Geological Congress with international participation, Abstract Book, Zagreb, pp 89–90.

Hohenegger, J., Rögl, F., Ćorić, S.,, Pervesle.r P, Lirer,. F. Roetzel, R., Scholger, R., Stingl, K., 2009. The Styrian Basin: a key to the Middle Miocene (Badenian/Langhian) Central Paratethys transgressions. Austrian Journal of Earth Science, 102, 102–132.

Hohenegger, J., Ćorić, S., Wagreich, M.,2014. Timing of the middle Miocene Badenian stage of the Central Paratethys. Geologica Carpathica, 65(1), 55-66. https://doi.org/10.2478/geoca-2014-0004

Holcová, K., 1999. Postmortem transport and resedimentation of foraminiferal tests: relations to cyclical changes of foraminiferal assemblages. PaleoPaleogeography, PaleoPaleoclimatology, PaleoPaleoecology 145(1-3), 157-182. https://doi.org/10.1016/S0031-0182(98)00100-X

Holcová, K., Doláková, N., Nehyba, S.,Vacek, F., 2018. Timing of Langhian bioevents in the Carpathian Foredeep and northern Pannonian Basin in relation to oceanographic, tectonic and climatic processes. Geological Quarterly, 62(1), 3-17. http://dx.doi.org/10.7306/gq.1399

Holcová, K., Kopecká, J., & Scheiner, F. (2019). An imprint of the Mediterranean middle Miocene circulation pattern in a satellite sea during the Langhian: A case study from the Carpathian Foredeep (Central Paratethys). PaleoPaleogeography, PaleoPaleoclimatology, PaleoPaleoecology, 514, 336-348. https://doi.org/10.1016/j.paleopaleo.2018.10.024

Horváth, F., Bada, G., Szafián, P., Tari, G., Ádám, A., Cloetingh, S., 2006. Formation and deformation of the Pannonian Basin: constraints from observational data. In: Gee DG, Stephenson RA (Eds.), European Lithosphere Dynamics. Geological Society, London, Memoirs 32, pp 191–206. https://doi.org/10.1144/GSL.MEM.2006.032.01.11

Horváth, F., Musitz, B., Balázs, A., Végh, A.,, Uhrin A.,, Nádor A., Koroknai, B., Pap, N., Tóth, T., Wórum, G., 2015. Evolution of the Pannonian Basin and its geothermal resources. Geothermics, 53, 328–352. https://doi.org/10.1016/j.geothermics.2014.07.009

Hrvatski geološki institut, 2009. Geološka karta Republike Hrvatske, M 1:300.000, Hrvatski geološki institut, Zavod za geologiju, Zagreb.

Hüsing, S. K., Cascella, A., Hilgen, F. J., Krijgsman, W., Kuiper, K. F., Turco, E., Wilson, D., 2010. Astrochronology of the Mediterranean Langhian between 15.29 and 14.17 Ma. Earth and Planetary Science Letters, 290(3-4), 254-269. https://doi.org/10.1016/j.epsl.2009.12.002

Chapman, M.R., 2010. Seasonal production patterns of planktic foraminifera in the NE Atlantic Ocean: implications for paleotemperature and hydrographic reconstructions. Paleoceanography 25, PA1101. http://dx.doi.org/10.1029/2008PA001708.

Incarbona, A., Jonkers, L., Ferraro, S., Sprovieri, R., Tranchida, G. 2019. Sea surface temperatures and paleoenvironmental variability in the Central Mediterranean during historical times reconstructed using planktic foraminifera. Paleoceanography and Paleoclimatology, 34(3), 394-408. http://dx.doi.org/10.1029/2018PA003529

Ivančič, K., Trajanova, M., Ćorić, S., Rožič, B., Šmuc, A., 2018. Miocene paleogeography and biostratigraphy of the Slovenj Gradec Basin: a marine corridor between the Mediterranean and Central Paratethys. Geologica Carpathica, 69, 528–544.

Jaramillo, C. A., Oboh-Ikuenobe, F. E.,1999. Sequence stratigraphic interpretations from palynofacies, dinocyst and lithological data of Upper Eocene–Lower Oligocene strata in southern Mississippi and

Alabama, US Gulf Coast. PaleoPaleogeography, PaleoPaleoclimatology, PaleoPaleoecology, 145(4), 259-302. https://doi.org/10.1016/S0031-0182(98)00126-6

John, C. M., Mutti, M., Adatte, T. (2003). Mixed carbonate-siliciclastic record on the North African margin (Malta)—coupling of weathering processes and mid Miocene climate. Geological Society of America Bulletin, 115(2), 217-229.

Kameo, K., 2002. Late Pliocene Caribbean surface water dynamics and climatic changes based on calcareous nannofossil records. PaleoPaleogeography, PaleoPaleoclimatology, PaleoPaleoecology 179(3-4), 211-226. https://doi.org/10.1016/S0031-0182(01)00432-1

Kocsis, L., Vennemann, T. W., Fontignie, D., Baumgartner, C., Montanari, A., 2008. Oceanographic and climatic evolution of the Miocene Mediterranean deduced from Nd, Sr, C e O isotope compositions of marine fossils and sediments. Paleoceanography, 23, PA4211. https:// doi.org/10.1029/2007PA001540.

Kocsis, L., Vennemann, T. W., Hegner, E., Fontignie, D.,Tütken, T., 2009. Constraints on Miocene oceanography and climate in the Western and Central Paratethys: O-, Sr-, and Nd-isotope compositions of marine fish and mammal remains. PaleoPaleogeography PaleoPaleoclimatology PaleoPaleoecology, 271(1), 117–129. http://dx.doi.org/10.1016/j.paleopaleo.2008.10.003

Kováč, M., Andreyeva-Grigorovich,A., Bajraktarević, Z., Brzobohatý, R., Filipescu, S., Fodor, L., Harzhauser, M., Nagymarosy, A., Oszczypko, N., Pavelić, D., Rög,l F., Saftić, B., Sliva, Ľ., Studencka, B., 2007. Badenian evolution of the Central Paratethys Sea: paleogeography, climate and eustatic sea-level changes. Geologica Carpathica 58, 579–606

Kováč, M., Halásova, E., Hudáčkova, N., Holcová, K., Hyžný, M., Jamrich, M., Ruman, A., 2018. Towards better correlation of the Central Paratethys regional time scale with the standard geological time scale of the Miocene Epoch. Geologica Carpathica, 69, 283–300.

Kováč, M., Márton, E., Oszczypko, N., Vojtko, R., Hók, J., Králiková, S., Plašienka, D., Klučiar, T.,Hudáčková, N., Oszczypko-Clowes, M., 2017. Neogene paleopaleogeography and basin evolution of the Western Carpathians, Northern Pannonian domain and adjoining areas. Global and Planetary Change, 155, 133-154. https://doi.org/10.1016/j.gloplacha.2017.07.004

Kovačić, M., Pavelić, D., 2017. Neogene stratigraphy of Slavonian Mountains. In: Kovačić M, Wacha L, Horvat M (Eds.), Field Trip Guidebook: Neogene of Central and South-Eastern Europe. Croatian Geological Society, Zagreb, pp 5–9.

Lukács, R., Harangi, S., Guillong, M., Bachmann, O., Fodor, L., Buret, Y., Dunkl, I., Sliwinski, J., von Quadt, A., Peytcheva, I., Zimmerer, M., 2018. Early to Mid-Miocene syn-extensional massive silicic volcanism in the Pannonian Basin (East-Central Europe): Eruption chronology, correlation potential and geodynamic implications. Earth-Science Reviews, 179, 1–19. https://doi.org/10.1016/j.earscirev.2018.02.005

Mackensen, A., Schumacher, S., Radke, J., Schmidt, D.N., 2000. Microhabitat preferences and stable carbon isotopes Yof endobenthic foraminifera: clue to quantitative reconstruction of oceanic new production? Marine Micropaleontology 40, 233–258. http://dx.doi.org/10.1016%2FS0377-8398(00)00040-2

Majewski, W., 2003. Water-depth distribution of Miocene planktic foraminifera from ODP Site 744, Southern Indian Ocean. The Journal of Foraminiferal Research 33(2), 144-154. https://doi.org/10.2113/0330144

Mandic, O., de Leeuw, A., Bulić, J., Kuiper, K.F., Krijgsman, W., Jurišić-Polšak, Z., 2012. Paleogeographic evolution of the Southern Pannonian Basin: $^{40}Ar/^{39}Ar$ age constraints on the Miocene continental series of Northern Croatia. International Journal of Earth Science, 101, 1033–1046. http://dx.doi.org/10.1007/s00531-011-0695-6

Mandic, O., Hajek-Tadesse, V., Bakrač, K., Reichenbacher, B., Grizelj A., Miknić, M., 2019a. Multiproxy reconstruction of the middle Miocene Požega paleolake in the Southern Pannonian Basin

(NE Croatia) prior to the Badenian transgression of the Central Paratethys Sea. Palaoegeography, PaleoPaleoclimatology, PaleoPaleoecology, 516, 203–219. http://dx.doi.org/10.1016/j.paleopaleo.2018.12.003

Mandic, O., Rundić, L.J., Ćorić, S., Pezelj, Đ., Theobalt, D., Sant, K., Krijgsman, W. ,2019c. Age and mode of the Middle Miocene marine flooding of the Pannonian Basin – constraints_from central Serbia. Palaios, 34, 71–95. https://doi.org/10.2110/palo.2018.052

Mandic, O., Sant, K., Kallanxhi, M.E., Ćorić, S., Theobalt, D., Grunert, P., de Leeuw, A., Krijgsman, W., 2019b. Integrated bio-magnetostratigraphy of the Badenian reference section Ugljevik in southern Pannonian Basin – implications for the Paratethys history (middle Miocene, Central Europe). Global and Planetary Change, 172, 374–395. https://doi.org/10.1016/j.gloplacha.2018.10.010

Marković, F., 2017. Miocene tuffs of the North Croatian Basin. Dissertation thesis, University of Zagreb.

Marković, S. B., Oches, E. A., Perić, Z. M., Gaudenyi, T., Jovanović, M., Sipos, G., Thiel, Ch., Buylaert J.P., Savić, S., Mccoy, W.D., Radaković, M.G., Marković, R.S., Gavrilov, M. B. (2021). The Požarevac loess–paleosol sequence: a record of increased aridity in the south-eastern margin of the Carpathian Basin during the last 350 ka. Journal of Quaternary Science, 36(8) 1436–1447

Matenco, L., Radivojević, D., 2012. On the formation and evolution of the Pannonian Basin: constraints derived from the structure of the junction area between the Carpathians and Dinarides. Tectonics, 31, TC6007. https://doi.org/10.1029/2012TC003206

McArthur J.M., Howarth R.J., Shields G.A. and Zhou Y. 2020. Strontium isotope stratigraphy, Chapter 7, p211 – p238. In: Gradstein F.M., Ogg J.G., Schmitz M.D. and Ogg G.M. A Geologic Time Scale, Elsevier B.V., Vol 1 of 2, 1357 pp. 2020.

McArthur, J. M., Howarth, R. J., Bailey, T. R., 2001. Strontium isotope stratigraphy: LOWESS version 3: best fit to the marine Sr-isotope curve for 0–509 Ma and accompanying look-up table for deriving numerical age. The Journal of Geology, 109(2), 155-170. https://doi.org/0.1086/319243

Methner, K., Campani, M., Fiebig, J., Löffler, N., Kempf, O., & Mulch, A. (2020). Middle Miocene long-term continental temperature change in and out of pace with marine climate records. Scientific reports, 10(1), 7959. https://doi.org/10.1038/s41598-020-64743-5

Modestou, S., Simon, D., Gutjahr, M., Marzocchi, A., Kouwenhoven, T. J., Ellam, R. M., & Flecker, R. (2017). Precessional variability of 87Sr/86Sr in the late Miocene Sorbas Basin: An interdisciplinary study of drivers of interbasin exchange. *Paleoceanography*, *32*(6), 531-552. https://doi.org/10.1002/2016PA003061

Moreno, R., Antolın, G., Reyes, A., Alvarez, P. 2004. Drying characteristics of forest biomass particles of Pinus radiata. Biosystems Engineering 88(1), 105-115. https://doi.org/10.1016/j.biosystemseng.2004.03.005

Munsterman, D. K., Brinkhuis, H., 2004. A southern North Sea Miocene dinoflagellate cyst zonation. Netherlands Journal of Geosciences, 83(4), 267-285. https://doi.org/10.1017/S0016774600020369

Murray, J. W.,2014. Ecology and paleopaleoecology of benthic foraminifera. Routledge, Washington, 408 pp.

Murray, J.W., 2006. Ecology and Applications of Benthic Foraminifera. Cambridge University Press, Cambridge, 426 pp.

Ohta, S., Kaiho, K., Takei, T., 2003. Relationship between surface-water temperature and ice-sheet expansion during the Middle Miocene. PaleoPaleogeography, PaleoPaleoclimatology, PaleoPaleoecology, 201(3-4), 307-320. https://doi.org/10.1016/S0031-0182(03)00617-5

Okada, H., McIntyre, A.,1979. Seasonal distribution of modern coccolithophores in the western North Atlantic Ocean. Marine Biology, 54(4), 319-328.

Ottens, J. J., Nederbragt, A. J., 1992. Planktic foraminiferal diversity as indicator of ocean environments. Marine Micropaleontology, 19(1-2), 13-28. https://doi.org/10.1016/0377-8398(92)90019-G

Pavelić, D., 2001. Tectonostratigraphic model for the North Croatian and North Bosnian sector of the Miocene Pannonian Basin System. Basin Research, 13, 359–376. http://dx.doi.org/10.1046/j.0950-091x.2001.00155.x

Pavelić, D., Kovačić, M., 2018. Sedimentology and stratigraphy of the Neogene rift-type (Pannonian Basin System, Croatia): a review. Marine Petrology Geolology, 91, 455–469. https://doi.org/10.1016/j.marpetgeo.2018.01.026

Pearson, P. N., Wade, B. S., 2009. Taxonomy and stable isotope paleoecology of well-preserved planktic foraminifera from the uppermost Oligocene of Trinidad. Journal of Foraminiferal Research 39(3), 191-217. https://doi.org/10.2113/gsjfr.39 3.191

Pezelj, D., Mandic, O., Ćoric, S., 2013. Paleoenvironmental dynamics in the southern Pannonian Basin during initial Middle Miocene marine flooding. Geologica Carpathica 64(1), 81-100. https:// doi.org/ 10.2478/geoca-2013-0006

Piller, W. E., Harzhauser, M., Mandic, O., 2007. Miocene Central Paratethys stratigraphy–current status and future directions. Stratigraphy, 4, 151-168.

Pin, C., Gannoun, A., Dupont, A., 2014. Rapid, simultaneous separation of Sr, Pb, and Nd by extraction chromatography prior to isotope ratios determination by TIMS and MC-ICP-MS. Journal of Analytical Atomic Spectrometry, 29(10), 1858-1870. https:// doi.org/ 10.1039/c4ja00169a

Popov, SV., Rögl, F., Rozanov, A.Y., Steininger, F.F., Shcherba, .IG., Kovac, M., 2004. Lithological-paleogeographic maps of Paratethys. In: CFS Courier Forschungsinstitut Senckenberg, pp 1–46.

Reynolds, L., Thunell, R.C., 1985. Seasonal succession of planktic foraminifera in the subpolar North Pacific. J. Foraminifer. Res. 15, 282–301.

Rögl, F., Spezzaferri, S., 2003. Foraminiferal paleoecology and biostratigraphy of theMühlbach section (Gaindorf Formation, Lower Badenian), Lower Austria. Annalen des Naturhistorischen Museums in Wien, 104A, 23-75.

Rögl, F., 1998. PaleoPaleogeographic considerations for Mediterranean and Paratethys seaways (Oligocene to Miocene). Annalen Naturhistorischen Museums in Wien, 99A, 279-310.

Rybár, S., Šarinová, K., Sant, K., Kuiper, K.F., Kováčová, M., Vojtko, R., Resiser, M.K., Fordinál, K., Theodoridis, V., Nováková, P., Vlček, T., 2019. New $^{40}Ar/^{39}Ar$, fission track and sedimentological data on a middle Miocene tuff occurring in the Vienna Basin: Implications for the north-western Central Paratethys region. Geologica Carpathica, 70, 386–404.

Sancetta, C., Villareal, T., Falkowski, P., 1991. Massive fluxes of rhizosolenid diatoms: a common occurrence?. Limnology and Oceanography, 36(7), 1452-1457.

Sant, K., Kuiper, K.F., Rybár, S., Grunert, P., Harzhauser, M., Mandic, O., Jamrich, M., Šarinová, K., Hudáčková, N., Krijgsman, W., 2020. $^{40}Ar/^{39}Ar$ geochronology using high sensitivity mass spectrometry: Examples from middle Miocene horizons of the Central Paratethys. Geologica Carpathica, 71, 166–182.

Sant, K., Palcu, D., Mandic, O., Krijgsman, W., 2017. Changing seas in the Early–Middle Miocene of Central Europe: a Mediterranean approach to Paratethyan stratigraphy. Terra Nova, 29, 273–281. https://doi.org/10.1111/ter.12273

Sant, K., Palcu, D.V., Turco, E,, Di Stefano, A., Baldassini, N., Kouwenhoven, T., Kuiper, K.F., Krijgsman, W., 2019. The mid-Langhian flooding in the eastern Central Paratethys: integrated stratigraphic data from the Transylvanian Basin and SE Carpathian Foredeep. International Journal of Earth Science, 108, 2209–2232. http://dx.doi.org/10.1007/s00531-019-01757-z

Sautter, L. R., Sancetta, C. 1992. Seasonal associations of phytoplankton and planktic foraminifera in an upwelling region and their contribution to the seafloor. Marine Micropaleontology, 18(4), 263-278.

Sautter, L. R., Thunell, R. C., 1991. Seasonal variability in the δ18O and δ13C of planktic foraminifera from an upwelling environment: sediment trap results from the San Pedro Basin, Southern California Bight. Paleoceanography, 6(3), 307-334. https://ui.adsabs.harvard.edu/link_gateway/1991PalOc...6..307S/doi:10.1029/91PA00385

Sen Gupta, B.K., Machain-Castillo, M.L., 1993. Benthic foraminifera in oxygen-poor habitats. Mar. Micropaleontol. 20, 183–201.

Shevenell, A. E., Kennett, J. P., Lea, D. W., 2008. Middle Miocene ice sheet dynamics, deep-sea temperatures, and carbon cycling: A Southern Ocean perspective. Geochemistry, Geophysics, Geosystems 9, Q02006, https://doi.org/10.1029/2007GC001736

Scheiner, F., Holcová, K., Milovský, R., & Kuhnert, H. (2018). Temperature and isotopic composition of seawater in the epicontinental sea (Central Paratethys) during the Middle Miocene Climate Transition based on Mg/Ca, δ18O and δ13C from foraminiferal tests. PaleoPaleogeography, PaleoPaleoclimatology, PaleoPaleoecology, 495, 60-71. https://doi.org/10.1016/j.paleopaleo.2017.12.027

Scheiner, F., Holcova, K., Milovský, R., Dolakova, N., & Rigova, J., 2019. Response of benthic foraminiferal communities to changes in productivity and watermass conditions in the epicontinental Paratethys during the Middle Miocene. Marine Micropaleontology 151, 101750. https://doi.org/10.1016/j.marmicro.2019.101750

Schiebel, R., Hemleben, C. 2017. Planktic foraminifers in the modern ocean. Springer, Berlin, 358 pp.

Schiebel, R., Bijma, J., Hemleben, C., 1997. Population dynamics of the planktic foraminifer Globigerina bulloides from the eastern North Atlantic. Deep Sea Research Part I: Oceanographic Research Papers, 44(9-10), 1701-1713. https://doi.org/10.1016/S0967-0637(97)00036-8

Schiebel, R., Hemleben, C., 2005. Modern planktic foraminifera. Paläontologische Zeitschrift, 79, 135–148. http://dx.doi.org/10.1007/BF03021758

Schildgen, T. F., D. Cosentino, G. Frijia, F. Castorina, F. €O. Dudas, A. Iadanza, G. Sampalmieri, P. Cipollari, A. Caruso, S. A. Bowring, and M. R. Strecker (2014), Sea level and climate forcing of the Sr isotope composition of late Miocene Mediterranean marine basins, Geochem. Geophys. Geosyst., 15, 2964–2983, doi:10.1002/2014GC005332.

Schmidt, D.N., Renaud, S., Bollmann, J., Schiebel, R., Theirstein, H.R., 2004a. Size distribution of Holocene planktic foraminifer assemblages: biogeography, ecology and adaptation. Marine Micropaleontology, 50, 319-338. https://doi.org/10.1016/S0377-8398(03)00098-7

Schmiedl, G., De Bovée, F., Buscail, R., Charriere, B., Hemleben, C., Medernach, L., Picon, P., 2000. Trophic control of benthic foraminiferal abundance and microhabitat in the bathyal Gulf of Lions, western Mediterranean Sea. Marine Micropaleontology 40 (3), 167–188. http://dx.doi.org/10.1016/S0377-8398(00)00038-4

Schmiedl, G., Pfeilsticker, M., Hemleben, C., Mackensen, A., 2004. Environmental and biological effects on the stable isotope composition of recent deep-sea benthic foraminifera from the western Mediterranean Sea. Marine Micropaleontology 51, 129–152. https://doi.org/10.1016/j.marmicro.2003.10.001.

Schulz, H. M., Bechtel, A.,Sachsenhofer, R. F., 2005. The birth of the Paratethys during the Early Oligocene: From Tethys to an ancient Black Sea analogue? Global and Planetary Change, 49(3-4), 163-176. https://doi.org/10.1016/j.gloplacha.2005.07.001

Sjoerdsma, P.G., Van der Zwaan, G.J., 1992. Simulating the effect of changing organic flux and oxygen content on the distribution of benthic foraminifera. Marine Micropaleontology, 19, 163–180. https://doi.org/10.1016/0377-8398(92)90027-H

Sosdian, S.M., Babila, T.L., Greenop, R., Foster, G.L., Lear, CH., 2020. Ocean Carbon Storage across the middle Miocene: a new interpretation for the Monterey Event. Nature, 11, 134. https://www.nature.com/articles/s41467-019-13792-0

Spezzaferri, S., 1995. Planktonic foraminiferal paleoclimatic implications across the Oligocene-Miocene transition in the oceanic record (Atlantic, Indian and South Pacific). PaleoPaleogeography, PaleoPaleoclimatology, PaleoPaleoecology, 114(1), 43-74. https://doi.org/10.1016/0031-0182(95)00076-X

Steinthorsdottir, M., Coxall, H.K., de Boer, A.M., Huber, M., Barbolini, N., Bradshaw, C.D., et al. (2021) The Miocene: The Future of the Past. Paleoceanography and Paleoclimatology ,36, e2020PA004037. https://doi.org/10.1029/2020PA004037

Triantaphyllou, M., Dimiza, M. D., Malinverno, E., Young, J. R. 2009. Evidence for a possible life-cycle association between Syracosphaera protrudens (Heterococcolithophore) and Syracosphaera pulchra HOL pirus type (Holococcolithophore). Journal of Micropaleopaleontology. 28(1), 1-6. https://doi.org/10.1144/jm.28.1.1

Turco, E., Hüsing, S., Hilgen, F., Cascella, A., Gennari, R., Iaccarino, S. M., Sagnotti, L. (2017). Astronomical tuning of the La Vedova section between 16.3 and 15.0 Ma. Implications for the origin of megabeds and the Langhian GSSP. Newsletters on Stratigraphy, 50(1), 1-29. http://doi.org/10.1127/nos/2016/0302

Utescher, T., Böhme, M., & Mosbrugger, V. (2011). The Neogene of Eurasia: Spatial gradients and temporal trends—The second synthesis of NECLIME. Palaeogeography, Palaeoclimatology, Palaeoecology, 304(3-4), 196-201.

Wade, B., Bown, P. R., 2006. Calcareous nannofossils in extreme environments: The Messinian Salinity Crisis, Polemi Basin, Cyprus. PaleoPaleogeography PaleoPaleoclimatology PaleoPaleoecology, 233, 271-286. https://doi.org/10.1016/j.paleopaleo.2005.10.007

Wells, P., Okada, H., 1997. Response of nannoplankton to major changes in sea-surface temperature and movements of hydrological fronts over Site DSDP 594 (south Chatham Rise, southeastern New Zealand), during the last 130 kyr. Marine Micropaleontology 32(3-4), 341-363. https://doi.org/10.1016/S0377-8398(97)00025-X

Williams, G. L., Brinkhuis, H. M. A. P., Pearce, M. A., Fensome, R. A., Weegink, J. W. 2004. Southern Ocean and global dinoflagellate cyst events compared: index events for the Late Cretaceous–Neogene. In Hine ,A. C., Feary , D. A., Malone, M. J. (eds.), Proceedings of the Ocean Drilling Program, Scientific Results, 189, College Station, Texas, Ocean Drilling Program, 2020, pp. 1-98.

Wilson, B., 2005. Planktic Foraminiferal Biostratigraphy and Paleo-Ecology of the Brasso Formation (Middle Miocene) at St. Fabien Quarry, Trinidad, West Indies. Caribbean Journal of Science, 41(4), 797-803. http://dx.doi.org/10.1127/0078-0421/2012/0015

Winter, A., Jordan, R., Roth, P.H.,1994. Biogeography of living coccolithophores in ocean waters. In: Winter, A., Siesser, W.G. (Eds.), Coccolithophores. Cambridge University Press, Cambridge, pp. 13–37.

Wright, J. D., Miller, K. G., Fairbanks, R. G., 1992. Early and Middle Miocene stable isotopes: Implications for Deepwater circulation and climate. Paleoceanography 7, 357–389, https://doi.org/10.1029/92PA00760

You, Y., Huber, M., Müller, R. D., Poulsen, C. J., Ribbe, J., 2009. Simulation of the middle Miocene climate optimum. Geophysical Research Letters, 36(4), L04702. https:// doi.org/ 10.1029/2008GL036571.

Young, J.R., Bown P.R., Lees J.A., 2017. Nannotax3 website. International Nannoplankton Association. https://www.mikrotax.org/Nannotax3

Zachos, J.,, Pagan.i M, Sloan, L., Thomas, E., Billups, K., 2001. Trends, rhythms, and aberrations in global climate 65 Ma to present. Science, 292, 686–693.

Zachos, J.C., Dickens, G.R., Zeebe, R.E., 2008. An early Cenozoic perspective on greenhouse warming and carbon-cycle dynamics. Nature, 451, 279–283. https://doi.org/10.1126/science.1059412

Zágoršek, K., Vávra, N., Holcová, K., 2007. New and unusual Bryozoa from the Badenian (Middle Miocene) of the Moravian part of the Vienna Basin (Central Paratethys, Czech Republic). Neues

Jahrbuch für Geologie und Paläontologie-Abhandlungen, 201-215. https:// doi.org/ 10.1127/0077-7749/2007/0243-0201

Zevenboom, D.,1995. Dinoflagellate cysts from the Mediterranean Late Oligocene and Miocene, 221 pp. Unpublished Ph. D. thesis, University of Utrecht, The Netherlands.

Zonneveld, K. A., Marret, F., Versteegh, G. J., Bogus, K., Bonnet, S., Bouimetarhan, I., Crouche, E., de Vernald, A., Elshanawanya,R., Lucy Esperc,E. O., Forkea, S., Grøsfjeldh, K., Henryd, M., Holzwartha,U., Kieltd,J. F., Kimi, So-Y., Ladouceurd, S., Ledud, D., Chena, L., Limogesd, A., Londeixj,L., Lud, S. H., Mahmoudk, M. S., Marinol, G., Matsuokam, K., Matthiesseng, J., Mildenhale, D.C., Mudiew, P., Neiln, H.L., Pospelovao, V., Qu, Y., Radid, T., Richerolp, T., Rochonp, A., Sangiorgil, F., Solignacs, S., Turonj, J. L., Verleyaq, T., Wangu, Y., Wang, Z., Young, M., 2013. Atlas of modern dinoflagellate cyst distribution based on 2405 data points. Review of PaleoPaleobotany and Palynology 191, 1-197. http://dx.doi.org/10.1016/j.revpalbo.2012.08.003

Zevenboom, D.,1995. Dinoflagellate cysts from the Mediterranean Late Oligocene and Miocene, 221 pp. Unpublished Ph. D. thesis, University of Utrecht, The Netherlands.

**Highlights**: 5*85 characters

- determination of two transgressive pulses of the Middle Miocene flooding in the Paratethys
- (1) shallow marginal sea strongly affected by freshwater input
- (2) deeper marginal sea with a developed seasonal stratification
- Plankton biostratigraphy coupled with geochronology/SIS ($^{87}Sr/^{86}Sr$) - the timing of individual floodings
- flooding phases - indicative of changes in circulation + sea-level changes